Transformation and sublimation of interstellar ices: insights from laboratory experiments and astronomical observations

Carvalho Santos, J. de

Citation

Carvalho Santos, J. de. (2025, July 2). *Transformation and sublimation of interstellar ices: insights from laboratory experiments and astronomical observations*. Retrieved from https://hdl.handle.net/1887/4252309

1. INTRODUCTION

If you wish to make a Ph.D. thesis from scratch, you must first invent the Universe.

It all began with the Big Bang. One second later, the Universe consisted of matter and radiation enmeshed in an extremely hot (10^{10} K) primordial soup. As it expanded and cooled, subatomic particles collided and formed the nuclei of the first atoms—hydrogen, helium, and traces of lithium and beryllium. This brief era of primordial nucleosynthesis ended within minutes, as the Universe became too cool for neutrons and protons to fuse. What remained was a dense, opaque plasma made of nuclei, free electrons, and light.

After 380 thousand years, the Universe had cooled enough for atomic nuclei and electrons to recombine, finally forming neutral atoms. This process, which itself generated a significant amount of radiation, allowed light and matter do decouple, rendering the Universe (momentarily) transparent. Light from that time is observed today as the cosmic microwave background (CMB)[1].

Within 200 million years, clumps of gas that accumulated in cooler areas of the Universe had grown massive enough to ignite nuclear fusion in their cores, giving rise to the first stars. It is through the life cycle of stars that most of the elements in the periodic table are formed—whether via nuclear fusion in stellar cores, via explosive events at the end of a star's life, or even from the collision of supermassive star core remnants known as neutron stars (Figure 1.1; Johnson 2019). These elements combine through a multitude of bonding arrangements to form molecules, some of which eventually coalesce into structures such as the planet we now call Earth.

Over the course of 4.5 billion years, the molecules that constitute the Earth underwent multiple cycles of destruction and reformation as the planet and its inhabitants were shaped into their current state. The work shown in this thesis is the result of the fraction of these elements and molecules that found their way to Earth, and ultimately became part of the cells that compose the writer's body, driving the exploration of the origins and fate of the other fractions that still permeate the interstellar medium.

To achieve this goal, this thesis combines laboratory simulations of interstellar ice processes—particularly, reactions and desorption—with observations of the gas surrounding protostars. The focus is on molecules containing carbon, hydrogen, oxygen, and sulfur, which, along with nitrogen and phosphorus, constitute the six major biogenic elements essential to virtually all life-related processes. By examining how such molecules form and evolve, this work provides insight into the chemical history of our own Solar System and beyond.

---

[1] Although the CMB was initially highly energetic, with the expansion of space its wavelength has increased, and its effective temperature has cooled off to just 2.7 K. After the CMB, the universe became opaque again due to light absorption by neutral atomic hydrogen—a period known as the Dark Ages. With the ignition of the first stars, hydrogen was reionized, making the universe transparent to light once more.

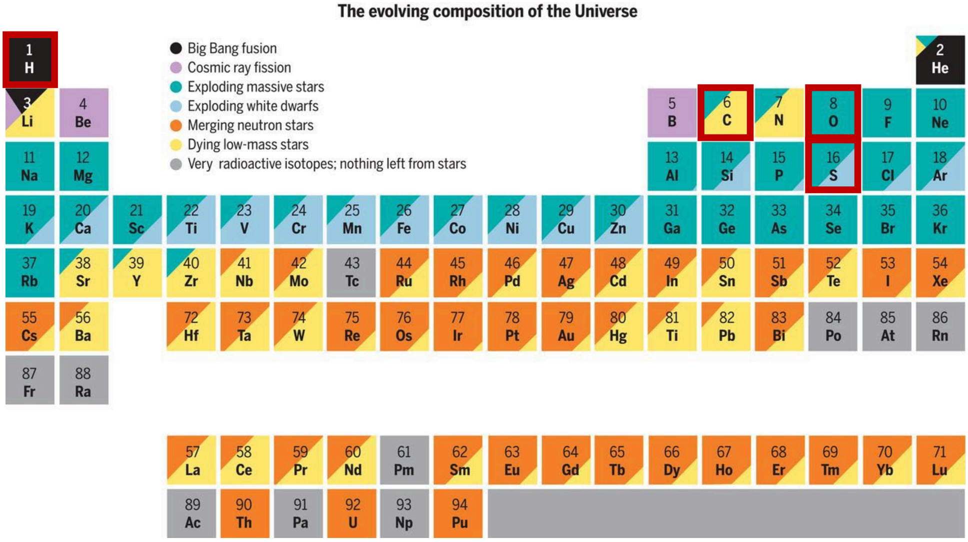

Figure 1.1: Periodic table of elements color-coded by their relative contributions from different nucleosynthesis sources. Carbon (C), hydrogen (H), oxygen (O), and sulfur (S) are particularly important for this thesis, and are highlighted in red. Artificially synthesized elements and those produced exclusively through the radioactive decay of long-lived nuclei are shaded in gray. Elements that do not occur naturally in the Solar System are omitted. Figure adapted from Johnson (2019).

1.1 Star and planet formation

To date, over 320 molecules have been detected in the interstellar medium or in circumstellar shells[2], with new detections increasing at an incredibly fast and possibly accelerating rate of ∼4.9 molecules per year (see McGuire 2022). The formation and destruction pathways of these molecules are shaped by the physical and chemical conditions of their environments, which in turn change dramatically throughout the different stages of star and planet formation (e.g., Herbst & van Dishoeck 2009). As a result, astrochemistry is inherently connected to the interstellar cycle of matter. The progression of this cycle depends on the mass of the star that is ultimately formed and can be broadly categorized into the evolution of low-mass and high-mass stars. In this thesis, the focus is primarily on low-mass stars due to their relevance to planetary systems capable of supporting life. Nevertheless, massive protostars are explored in Chapters 8 and 9, and therefore their formation is also briefly addressed.

1.1.1 Low-mass stars

Low-mass stars (<2 $M_\odot$) are the prevalent type of stars in the Galaxy and, consequently, the most frequent hosts of planetary systems. Their long main-sequence lifetimes provide the extended timescales thought to be necessary for life to emerge (i.e., $\sim 10^9$ yr, based on geological records tracing Earth's earliest organisms; Hol-

---

[2] https://cdms.astro.uni-koeln.de/classic/molecules

land 1997; Schopf 1993, 1994). As such, these stars are key to understanding the chemical evolution of planet-forming regions, and are frequently the objects of astrochemical studies. Figure 1.2 (Öberg & Bergin 2021) illustrates the different stages of star and planet formation in low-mass systems. It begins with dense molecular clouds, which are inhomogeneous structures measuring $2 - 15$ pc and with typical densities of $\sim 10^2 - 10^4$ cm^{-3} and temperatures of $\sim 10 - 20$ K (Bergin & Tafalla 2007). Within these clouds, there are substructures of even higher densities ($\sim 10^6$ cm^{-3}) called cores, with scales of $\sim$0.1 pc and where temperatures typically remain at $8-12$ K (Bergin & Tafalla 2007). When these cores accumulate sufficient mass, gravitational forces overtake thermal and magnetic pressures, as well as turbulence, causing the core to collapse and form a protostar. Centrally concentrated dense cores that are fated to collapse, but have not yet done so, are called prestellar cores.

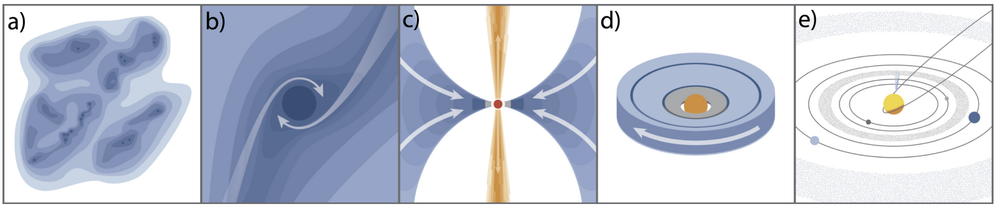

Figure 1.2: Schematic of the star- and planet-formation stages in low-mass systems. a) Dense cores form within molecular clouds. (b) These cores start to collapse under gravity to form a protostar. (c) As the protostar emerges, remnant cloud material continues to accrete by funneling through a circumstellar disk, while outflows and jets remove angular momentum from the system. (d) The envelope gradually dissipates, leaving behind a pre-main-sequence star surrounded by a protoplanetary disk. (e) After the disk material is depleted through accretion and dispersal, a planetary system remains. Figure from Öberg & Bergin (2021).

Once a protostar is born, it continues to accrete material from the surrounding envelope, which in turn experiences positive temperature and density gradients towards the accreting star. Due to the conservation of angular momentum, a portion of this material settles in a disk around the star (Tobin & Sheehan 2024). Angular momentum is further transferred out of the system via protostellar outflows and jets, while the disk facillitates accretion by chanelling matter onto the star. Over time, the star and disk continue to accrete mass as the surrounding envelope gradually dissipates, eventually dispersing completely within timescales of $\sim$10^6 yr. This process leaves behind a pre-main-sequence star surrounded by a Keplerian disk (Williams & Cieza 2011). This remaining structure, known as a protoplanetary disk, serves as the birthplace of planets and planetesimals—though recent evidence points to the onset of giant planet formation taking place as early as the embedded protostellar phases (Harsono *et al.* 2018; Tychoniec *et al.* 2020). Eventually, the disk material is completely depleted through accretion and dispersal, leaving behind a planetary system that may continue to evolve through collisions between its constituent bodies.

1.1.2 High-mass stars

In contrast to low-mass stars, high-mass stars ($\gtrsim$4 M$_\odot$) form on much shorter timescales ($\sim 10^4 - 10^5$ yr) and are typically located farther away ($d \gtrsim 1$ kpc), making their observation and the development of a formation paradigm more challenging (Beuther *et al.* 2007; Mottram *et al.* 2011). Several models have been proposed to explain massive star formation, with the two most prominent ones being a core accretion model, which is a scaled-up version of the model for low-mass stars, and the competitive accretion model, where protostellar seeds form through gravitational collapse and grow by tidally-modified Bondi-Hoyle accretion[3] (Bonnell & Bate 2006; Tan *et al.* 2014; Beuther *et al.* 2025). In this latter scenario, the gas is initially not gravitationally bound to any individual star, and the protostellar seeds compete for the mass available within the clump. Still, no clear consensus has been reached on the dominant mechanism driving massive star formation, with alternative (though less likely) scenarios, such as the merging of low-mass protostars, also being proposed (e.g., Bonnell *et al.* 1998).

Due to the shorter timescales of high-mass star formation, these stars do not exhibit visible pre-main-sequence phases[4]. Nonetheless, like their low-mass counterparts, massive protostars originate within clouds and undergo an embedded phase during which they heat their surrounding envelopes, giving rise to regions known as hot cores (Kurtz *et al.* 2000). Additionally, massive protostars are predicted to host disks where planets may form via gravitational instability (Boss 1997), though their short main-sequence lifespans are too brief to support the emergence of life.

1.2 Interstellar chemistry

As matter progresses through the different stages of star and planet formation—from clouds to protostars, to protoplanetary disks, and eventually planetary systems—it encounters a wide range of physical conditions (e.g., densities, temperatures, radiation fields) that can affect its molecular composition and distribution (Herbst & van Dishoeck 2009). Understanding the physicochemical processes at play in these environments, and consequently how chemistry evolves across these stages, is essential not only for interpreting observations but also for accurately predicting the outcomes of planet formation.

1.2.1 Gas vs ice reactions

Interstellar chemistry can be broadly separated into two different types of processes: gas-phase reactions and solid-phase reactions. In the former case, the low densities typical of most phases of star and planet formation inhibit three-body reactions of the form $A + B + C \rightarrow ABC^{\star} \rightarrow AB + C$, which require densities $\gtrsim 10^{13}$ cm^{-3}. Such conditions are only found in a few exceptionally dense environments, such as the atmospheres of AGB stars and the inner midplanes of protoplanetary disks. This limitation has significant implications for gas-phase chemistry: three-body reactions assist in the stabilization of the reaction product (AB) by having the third body (C) carry away the bond formation energy. In their absence, many systems must rely on alternative stabilization mechanisms, such as the emission of a photon or an electron, which are often inefficient. As a result, gas-phase reactions are constrained in their ability to form chemical bonds (Herbst & Klemperer 1973). Some bond-rearrangement

---

[3] Bondi-Hoyle accretion describes the spherical accretion onto a compact object moving through a uniform gas free of self gravity.

[4] Intermediate-mass cases ($2\mathrm{M}_{\odot} \lesssim \mathrm{M}_{\star} \lesssim 15\mathrm{M}_{\odot}$) are an exception, as pre-main-sequence stars in this range are observed and classified as Herbig Ae/Be (Brittain *et al.* 2023).

gas-phase reactions, of the form $A + BC \rightarrow AB + C$, can proceed efficiently because the excess energy is carried by the C product, eliminating the need for radiative stabilization. Ion-molecule reactions are an example of bond-rearrangement processes that play an important role in astrochemical networks, primarily because they are typically exothermic, and can proceed at high rates even at temperatures as low as 10 K due to long-range charge interactions between the reactants (van Dishoeck 2014; Öberg & Bergin 2021). For ions reacting with symmetric molecules with no permanent dipoles, the charge interactions occur via induced dipoles and rates are temperature independent, typically around 10^{-9} cm^{-3} s^{-1}. For neutral species with a permanent dipole, reaction rates are temperature dependent and can be enhanced by one to two orders of magnitude at low temperatures. In addition, neutral-neutral routes involving radicals as reactants can contribute significantly to form certain species, such as H_2O (when $T_{\rm gas} > 400$ K; Wagner & Graff 1987) and a few organic molecules (when in cold environments, Shannon *et al.* 2013; Balucani *et al.* 2015). Nonetheless, generally speaking, gas-phase reactions are less effective at driving chemical complexity in space.

In solid-phase reactions, on the other hand, the substrate (consisting of interstellar dust grains or frozen molecular layers coating these grains) act as the third body through which the excess energy from product formation can be dissipated, thus stabilizing the reaction products. In fact, abundant species such as H_2 and CH_3OH can only be attributed to solid-phase formation mechanisms, as their gas-phase formation is either highly inefficient or entirely prohibitive due to the inability to stabilize the reaction products (Geppert 2006; Vidali 2013). Additionally, these grains are typically at very low temperatures (<10 K in prestellar cores and <30 K in the more extended regions, like the outskirts of starless cores; Crapsi *et al.* 2007; Pagani *et al.* 2007). Under such conditions, sticking coefficients are nearly unity, meaning that most molecules—except for H_2 and He—will readily freeze out onto dust grains upon contact. As a result, these grains act as chemical reservoirs, facilitating encounters among reactants and promoting a rich solid-state chemistry. Given the key role played by ices in driving interstellar chemical complexity, this thesis focuses on solid-state phenomena and its contribution to the chemical evolution of the interstellar medium.

1.2.2 Ice processes

Once an atom or molecule adsorbs onto a dust grain, it can undergo three different types of processes: (i) desorption, (ii) diffusion, and (iii) reaction. An overview of these processes is provided in Figure 1.3.

The first process, desorption, occurs when a species overcomes its binding energy ($E_{\rm bind}$) to the surface and is released into the gas phase. Sources of energy that can lead to desorption include thermal heating (e.g., from a protostar), energetic particles such as UV photons, or the excess heat released by highly exothermic reactions.

The second process, diffusion, involves the movement of species across the grain surface upon overcoming their diffusion energy barrier ($E_{\rm diff}$). Diffusion can proceed via thermal hopping—when a species has enough energy to overcome the diffusion barrier classicaly—or via quantum tunneling through the barrier. Some light species (namely, H and O atoms) have been suggested to diffuse efficiently via quantum tunneling under specific conditions (e.g., at very low temperatures of $\lesssim$10 K, and on relatively smooth surfaces like polycristalline water ice; Congiu *et al.* 2014; Kuwahata *et al.* 2015). However, for most astrophysical contexts, thermal hopping is expected to

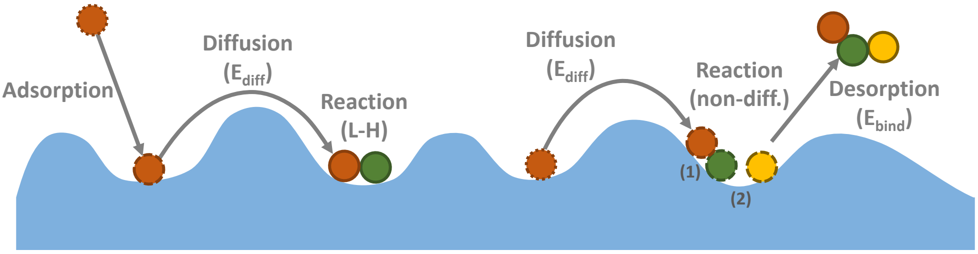

Figure 1.3: Illustration of the various processes experienced by chemical species on icy grain surfaces. The chronological order of events is indicated by species with dotted contours, followed by dashed contours, and finally solid-line contours. In one scenario, a species adsorbs onto the ice and diffuses by overcoming its diffusion energy (E_{diff}) until it encounters another molecule in a different binding site, where they react via the Langmuir-Hinshelwood (L-H) mechanism. In another scenario, a species diffuses to a new binding site and reacts via L-H with a second species (event denoted as (1) in the figure). The newly formed molecule then undergoes a second reaction (event (2)), forming a more complex species via the non-diffusive mechanism. The excess heat released from event (2) allows the molecule to overcome its binding energy (E_{bind}) and desorb from the ice.

dominate. Consequently, the mobility of a species is highly temperature-dependent, with most molecules remaining immobile at the low temperatures typical of prestellar environments.

The third process, reaction, takes place when species encounter one another under conditions conducive to chemical reactions. These have been historically thought to proceed through three primary mechanisms: Langmuir-Hinshelwood, Eley-Rideal, and hot atom. In the Langmuir-Hinshelwood mechanism, both reactants are thermalized on the grain surface, diffuse, meet, and react. The Eley-Rideal mechanism involves one reactant remaining stationary on the surface while another from the gas phase collides with it, triggering a reaction. In the hot-atom mechanism, a non-thermalized species briefly diffuses across the surface before encountering another molecule and reacting. In astrophysical ices, thermalization typically occurs on much shorter timescales than chemical reactions, rendering the hot atom mechanism largely irrelevant. The Eley-Rideal mechanism could potentially play a role under conditions of high surface coverages or low surface mobility (Cuppen *et al.* 2017)—conditions that can arise during events like the catastrophic CO freeze-out in prestellar cores (see Section 1.3.1). For most astrophysical environments, however, the Langmuir-Hinshelwood mechanism is thought to dominate among the three.

While diffusion has long been considered the standard scenario in astrochemical models and is a key limiting factor for chemical reactions, its absence does not entirely preclude molecule formation. At the extremely low temperatures typical of prestellar cores and the cold envelopes of protostars ($\lesssim$10 K), only atomic hydrogen can diffuse efficiently. Under such conditions, hydrogenation reactions are expected to dominate, producing simple species such as CH_4, NH_3, and CH_3OH from C, N, and CO. The formation of more complex species, however, requires that radical-radical and radical-molecule associations become competitive with the hydrogenation of these radicals. In a diffusive scenario, these conditions would only be met at $T \gtrsim 20$ K, where radicals become mobile. Yet, gas-phase observations towards cold interstellar environments have revealed the presence of complex organic molecules (COMs) such as acetaldehyde (CH_3CHO), methyl formate (CH_3OCHO), and dimethyl ether (CH_3OCH_3) (Öberg *et al.* 2010a; Bacmann *et al.* 2012; Cernicharo *et al.* 2012; Vastel *et al.* 2014), challenging this view. Given that these COMs are likely formed via solid-state chemistry, such findings suggest that diffusion is not the sole pathway for the formation of larger molecules in ices. To explain these observations, Jin & Garrod (2020) proposed a new non-diffusive mechanism—inspired in part by experimental results (e.g., Fedoseev *et al.* 2015a, 2017)—in which radicals react with nearby molecules to produce complex organics. In this scenario, the initial radical formation might proceed, for instance, through the hydrogenation of a closed-shell species via a standard Langmuir-Hinshelwood process, but the subsequent formation of complex organics occurs without requiring the radicals to be mobile. This non-diffusive mechanism is relevant to both bulk-ice and surface-ice reactions, and is likely responsible for much of the chemistry under molecular cloud conditions explored in this thesis (for which $T \leq 20$ K).

Regardless of whether reactions proceed via diffusive or non-diffusive mechanisms, astrophysical ice chemistry relies heavily on atoms and radicals, with only a limited number of feasible reactions involving strictly closed-shell species (such as the formation of ammonium and hydronium salts; e.g., Theule *et al.* 2011; Mispelaer *et al.* 2012; Loeffler *et al.* 2015; Bergner *et al.* 2016). Open-shell species can populate ices through adsorption from the gas phase or via in-situ formation. In the latter case, radicals can form within the ice through "non-energetic" processes, such as atom addition and abstraction reactions (e.g., Linnartz *et al.* 2015), or via molecular dissociation induced by energetic particles like UV photons and electrons (e.g., Öberg 2016). While energetic pathways are certainly relevant for generating radicals in ices, this thesis primarily focuses on non-energetic processes, which are thought to dominate under the shielded conditions characteristic of molecular clouds.

The low temperatures in astrophysical ices suppress endothermic reactions, thus only exothermic reactions (i.e., with a negative enthalpy change; $\Delta H < 0$) can proceed in the environments explored in this thesis. When these reactions have an activation energy barrier (E_a), they can proceed via either thermal hopping or quantum tunneling (Figure 1.4)—similar to the case of diffusion. In most astrochemical contexts, tunneling rates ($k_{\rm tunn}$) are described by using the Wentzel-Kramers-Brillouin (WKB) approximation[5] and assuming a rectangular barrier (Cuppen *et al.* 2017):

$$k_{\rm tunn} = \nu \exp\left(-\frac{2a}{h}\sqrt{2\mu E_{\rm a}}\right), \tag{1.1}$$

where ν is an attempt frequency (see, e.g., Cuppen *et al.* 2017), a is the width of the barrier, h is the Planck's constant, μ is the effective mass of the system, and $E_{\rm a}$ is the reaction energy barrier. Quantum tunneling becomes particularly relevant for light species such as H atoms, and is thought to dominate hydrogen addition and abstraction reactions in clouds and prestellar cores, where the classical solution is not thermally viable (e.g., Cuppen *et al.* 2017 and references therein). Notably, the efficiency of quantum tunneling decreases significantly when a species is replaced by its heavier

---

[5] The WKB method approximates a non-linear second order ordinary differential equation (in this case, the Schrödinger equation), which has no analytical solution, by assuming a slowly varying potential. In the context of tunneling it works by assuming the wavefunction to be an exponential function that is semiclassicaly expanded and with either amplitude or phase taken to be slowly changing relative to the de Broglie wavelength.

isotope. This phenomenon, known as the kinetic isotope effect, arises because the heavier isotope tunnels less efficiently through the barrier than its lighter counterpart (see equation 1.1). In the case of hydrogen, the twofold increase in mass from protium ($^{1}_{1}$H) to deuterium ($^{2}_{1}$H) results in a particularly pronounced effect, which was leveraged in Chapter 2 of this thesis as a tool to pinpoint the contributions of specific reaction pathways to methanol ice formation.

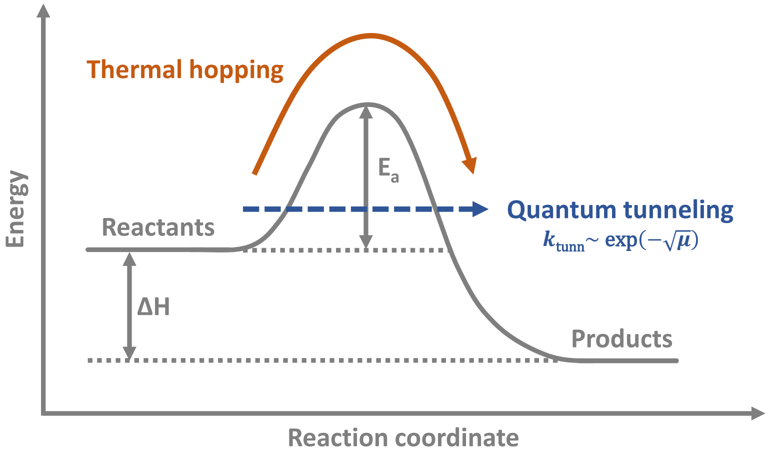

Figure 1.4: Illustration of the energy landscape along the reaction coordinate for an exothermic reaction ($\Delta H < 0$) with an activation energy (E_a). The activation barrier can be overcome through thermal hopping or quantum tunneling. Tunneling rates (k_{tunn}) are heavily dependent on the effective mass of the system (μ, see equation 1.1), giving rise to the kinetic isotope effect.

In the cases where quantum tunneling is inefficient (e.g., for heavier species), any activation barrier must be overcome through thermal hopping, making the reaction temperature dependent. In fact, even for barrierless reactions or those that proceed via tunneling, the temperature of the environment still influences how efficiently a reaction can occur. This is because temperature affects the diffusion and desorption rates of the reactants, which in turn influence how often they encounter one another and how long they remain in proximity before diffusing away. At higher temperatures, increased diffusion can enhance the likelihood of encounters among reactants, but the reduced residence time of reactants in each other's vicinity may be insufficient for the reaction to occur (Cuppen *et al.* 2017). Even in low-temperature environments, where only atomic hydrogen can diffuse, temperature remains a key factor in chemical networks. It directly influences the efficiency of hydrogenation reactions, which not only generate the simple species that constitute the bulk of the ice but also acts as the main trigger of non-diffusive chemistry by producing radicals that drive the formation of complex molecules.

1.3 Chemical evolution through star and planet formation

Interstellar clouds, where stars form, are composed of approximately 99% gas by mass, with elemental abundances dominated by hydrogen ($\sim$90% by number) and helium ($\sim$8%). All other elements in the periodic table are present in significantly lower quantities. For instance, elemental abundances of oxygen, carbon, and nitrogen—the next most abundant elements—correspond to 4.9×10^{-4}, 2.7×10^{-4}, and 6.8×10^{-5} relative to hydrogen, as derived from the Solar photosphere (Asplund *et al.* 2009), with minimal variation expected for the interstellar medium. Dust accounts for only $\sim$1% of the total mass of clouds, and is composed of silicates and carbonaceous material (Draine 2003; Chiar *et al.* 2013; Jones *et al.* 2013). Despite its small mass fraction, as discussed in the previous sections, dust plays a crucial role in the chemical evolution of star- and planet-forming regions by promoting a rich solid-state chemistry. The resulting chemical structures of molecular clouds and protostellar envelopes are briefly outlined in this Section. Here, we focus on the chemical evolution of low-mass star-forming systems, and refer to them as protostars for simplicity.

1.3.1 Prestellar phase

Figure 1.5 shows the chemical evolution of gas and ices along the prestellar phase. In the earliest stages of star formation—the diffuse cloud phase—densities are low ($\sim10^2$ cm^{-3}) and temperatures range from $\sim$30−100 K (e.g., Snow & McCall 2006). These regions are surrounded by diffuse atomic gas that provides some shielding to the radiation, allowing the interstellar radiation field to be sufficiently attenuated for molecular hydrogen to form in significant amounts ($>$ 10% of the hydrogen fraction). Elements with lower ionization potentials, such as carbon, remain predominantly in their ionized form. As these clouds become more compact, the interstellar radiation field is further attenuated, allowing ionized carbon to transition to its neutral state or partake in ion-molecule reactions to form CO efficiently (van Dishoeck & Black 1986). This marks the start of the translucent cloud stage, characterized by densities of $\sim10^3$ cm^{-3} and visual extinctions of $A_V \sim 1 - 2$ mag. In this stage, the dominant carbon reservoir is no longer C^+, as it is progressively converted into the its neutral atomic and molecular forms. With increasing compaction and extinction, a sufficiently thick CO column builds up to allow self-shielding against interstellar radiation (van Dishoeck & Black 1988). This leads to a dramatic increase in the CO formation efficiency, effectively locking up most of the available carbon. This transitions defines the dense molecular cloud stage, characterized by densities $> 10^4$ cm^{-3}, visual extinctions of $A_V \sim 5 - 10$ mag, and temperatures of $\sim 10 - 50$ K (Snow & McCall 2006). At even higher densities and extinctions within the cloud, gaseous nitrogen atoms undergo neutral-neutral reactions to form N_2 (Pineau des Forets *et al.* 1990; Gerin *et al.* 1992b), effectively sequestering most of the volatile nitrogen.

Ices begin to form early in the evolution of a cloud, once extinction levels reach a few mag (e.g., Whittet *et al.* 2013). At this stage, atomic and molecular oxygen on the surface of dust grains are efficiently hydrogenated to produce H_2O ice (Tielens & Hagen 1982; Hiraoka *et al.* 1998; Mokrane *et al.* 2009; Dulieu *et al.* 2010; Ioppolo *et al.* 2010; Cuppen *et al.* 2010)—a process so efficient that most of the available volatile oxygen becomes locked into it. Simultaneously, interactions between CO and OH on

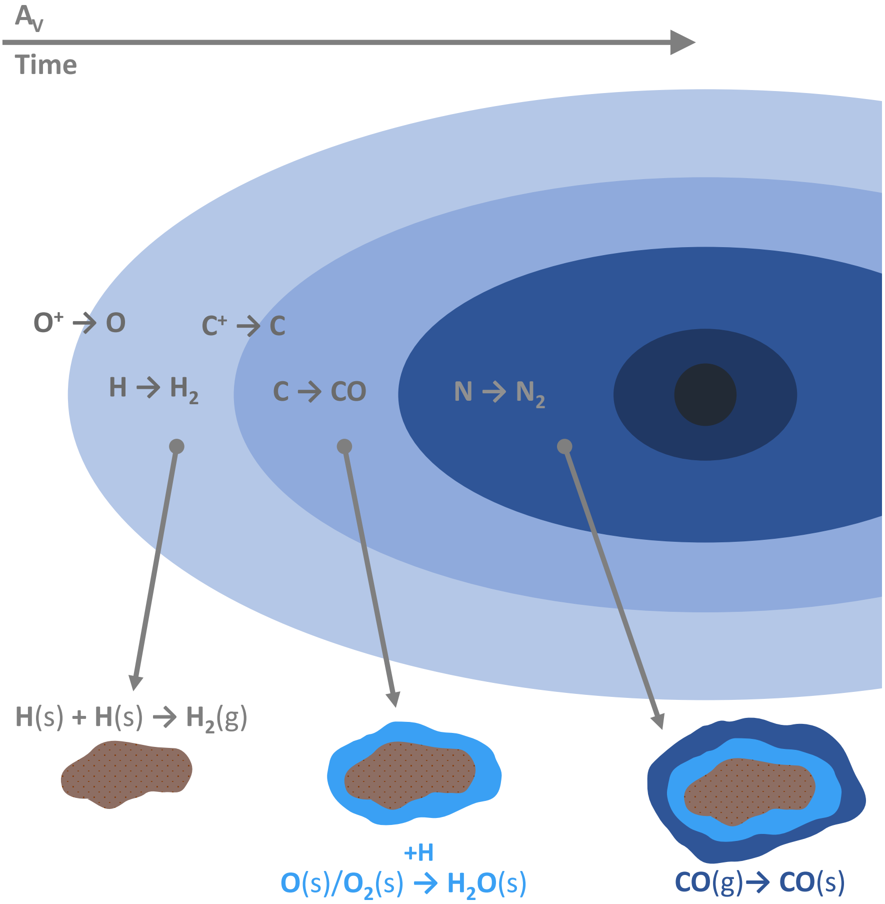

Figure 1.5: Illustration of the chemical evolution during the cloud stages preceding star formation. Gas-phase species are labeled with (g), while species in the solid are labeled with (s). The top arrow represents increasing cloud depth (corresponding to greater extinction) or time elapsed since the start of the compaction of diffuse cloud material. Adapted from Öberg & Bergin (2021).

dust grains lead to the formation of CO_2 (Ioppolo *et al.* 2011; Garrod & Pauly 2011). Other, less abundant species such as NH_3, CH_4, and H_2S also form via hydrogenation reactions on dust grains (respectively, of N, C, and S; e.g., Garrod *et al.* 2007; Garrod & Pauly 2011; Linnartz *et al.* 2015). The bulk of these molecules are produced on similar timescales as H_2O, coexisting as mixtures within a water-rich ice. However, small differences in their adsorption timescales, reactant mobility, and relative gas-phase abundances of their precursors may lead to local differences in ice mixing ratios.

Closer to the cloud core, once densities and extinction levels become sufficiently high ($> 10^5$ cm^{-3}, $A_V \geq 9$ mag), gas-phase CO begins freezing out onto dust grains at a rate that surpasses H-atom-activated surface reactions. This leads to the buildup of a CO-rich ice layer on top of the existing H_2O-rich one, a process known as catastrophic CO freeze-out (e.g., Pontoppidan 2006; Boogert *et al.* 2015). Within this ice layer, CO interacts with hydrogen atoms to form CH_3OH, the simplest COM (Watanabe &

Kouchi 2002; Fuchs *et al.* 2009; and Santos *et al.* 2022b—Chapter 2 of this thesis). Similarly, gaseous N_2 is expected to freeze-out around the same time or slightly later than CO (e.g., Öberg *et al.* 2005; Bisschop *et al.* 2006; Nguyen *et al.* 2018), leading to N_2 ice that is either mixed with or on top of CO ice. This results in a stratified ice structure, with a water-rich layer beneath a CO-rich counterpart, each containing additional molecular components in complex mixtures. Throughout the cloud stage, radicals are produced via atom-induced reactions (Linnartz *et al.* 2015; Chuang *et al.* 2016) or through energetic processing by cosmic rays, secondary electrons, or low-level UV fields generated by electronically-excited H_2 molecules (Prasad & Tarafdar 1983; Öberg 2016). Some of these radicals will form complex species via the non-diffusive mechanism (Jin & Garrod 2020), but a fraction will remain unreacted within the ice, and later will take part in a rich diffusive chemistry when heated in the envelopes surrounding protostars. The resulting main constituents of interstellar ices are shown in Figure 1.6, whose interactions drive the formation of even more complex molecules, which are the main topic of Chapters 4, 6, and 7 of this thesis.

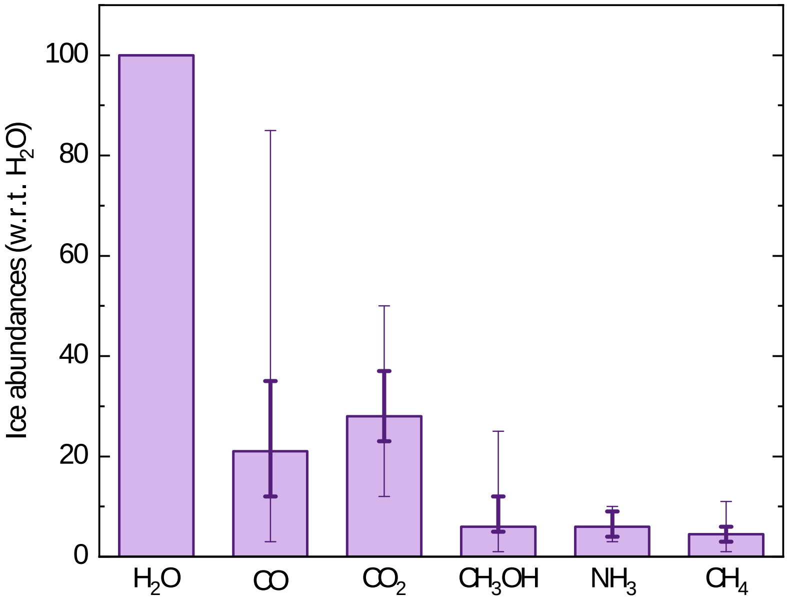

Figure 1.6: Median bulk abundances of the main components of interstellar ices observed towards low-mass protostars. The values are normalized to the most abundant ice species, water, with thick error bars representing the lower and upper quartiles of the detections, and thin error bars corresponding to the full range of detections. For CO and CH_3OH, the lower bounds of the full range of observations (thin errors) correspond to observed upper limits. Figure adapted from Öberg (2016), based on data summarized by Boogert *et al.* (2015).

1.3.2 Protostellar phase and beyond

Figure 1.7 shows the chemical evolution of ices along the protostellar phase. With the gravitational collapse of the prestellar core, a protostar emerges, surrounded by a large envelope of infalling cloud material. This protostar creates a temperature gradient that increases inwards, triggering a range of chemical and physical processes

(Herbst & van Dishoeck 2009). In the outer envelope (thousands of au from the central protostar), conditions remain similar to those of prestellar cores (with $T < 20$ K), and ice chemistry proceeds as a continuation of the previous prestellar stage. Closer to the protostar, increasing temperatures gradually enable molecules to become mobile, triggering a diffusive chemistry regime that leads to the production of a wide range of organic molecules (Garrod *et al.* 2008). Species also begin to desorb from the ice, with more volatile molecules (such as N_2, CO, and CH_4) sublimating at larger distances from the protostar, unless trapped within less volatile ice matrices. Sublimation alters the pool of available reactants in both the solid and gas phases, affecting the chemistry taking place in each. In particular, the sublimation of methane (at $\sim 20 - 30$ K) has been proposed to initiate a network of gas-phase reactions in warm protostellar envelopes, leading to the formation of carbon-chain species in a process known as warm carbon chain chemistry (WCCC; Sakai & Yamamoto 2013).

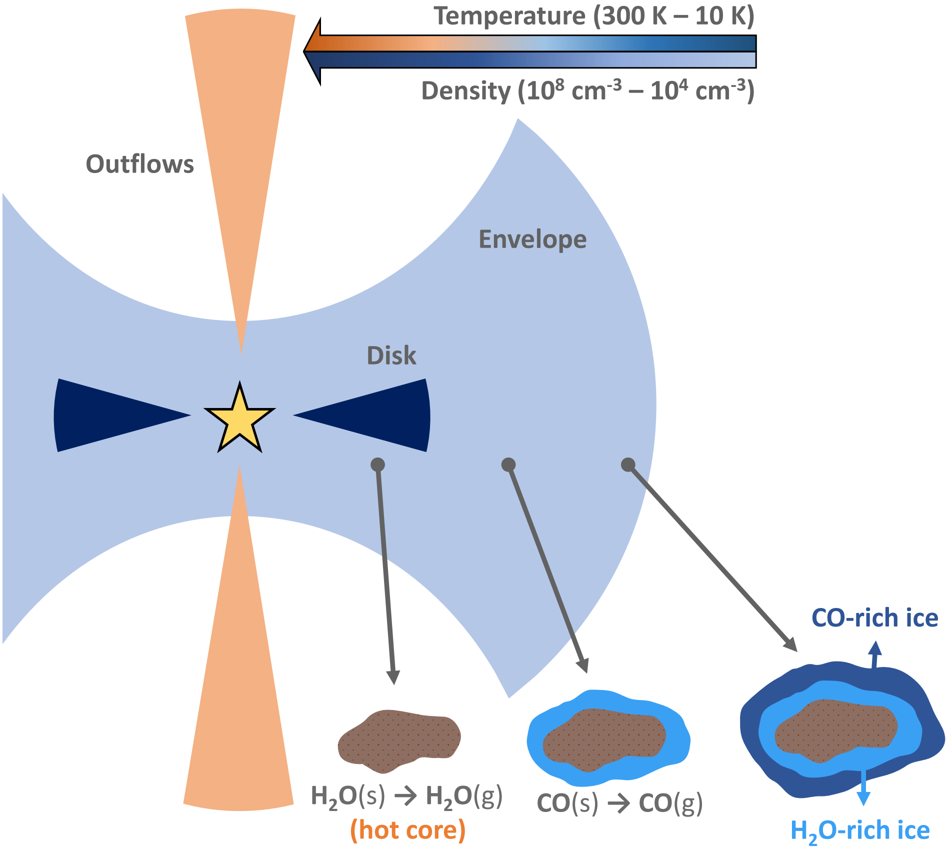

Figure 1.7: Illustration of the chemical structure of protostellar envelopes. As in Figure 1.5, (g) denotes gas-phase species, while (s) denotes solid-state species. As dust grains move closer to the protostar, rising temperatures drive diffusion, reactions, and desorption, with more volatile species sublimating at greater distances than less volatile ones—unless trapped. Where temperatures exceed 100 K, water ice and volatile COMs sublimate, giving rise to the hot core region. Figure adapted from Herbst & van Dishoeck (2009).

Within the region where temperatures exceed 100 K (at tens of au from the protostar during the embedded phases), the entire volatile ice reservoir sublimates, releasing its constituents into the gas phase. These regions, whose boundaries are defined by the sublimation of water ice, are often called hot corinos in low-mass protostars and hot cores in high-mass counterparts. Here, we use "hot core" as an umbrella term encompassing both. Hot cores are excellent environments to investigate ice composition, as molecules initially formed in ices become detectable through gas-phase techniques—which are much more sensitive and suffer less from line confusion than solid-state observations. However, hot cores may also undergo further chemical evolution (Caselli & Ceccarelli 2012), meaning that gas-phase observations towards such regions may not always directly reflect the original ice composition. Whether they do depends on the molecule and its chemical timescales. Observations of water, for instance, indicate a high degree of inheritance from the prestellar stage, with its gas-phase abundances in warm protostellar envelopes closely mirroring its icy precursors (Jensen *et al.* 2021; Slavicinska *et al.* 2024). In addition to thermal sublimation, ices in protostellar envelopes might also desorb as a result of shocks, for instance from the interactions with protostellar outflows (e.g., Arce *et al.* 2008; Lefloch *et al.* 2017).

Already during the embedded protostellar phases, disks may form at scales similar to those of the hot core. Initially, these disks are expected to be hot, potentially fully dissociating any molecule into its atomic constituents. Over time, however, the centrifugal radius of the disk expands, and infalling material from larger radii start to supply the disk. There is an ongoing discussion regarding the extent to which the material in these disks is inherited from the prestellar and protostellar phases versus being reset during the disk stage. In general, a combination of both is required to explain observational evidence from protostellar disks, as well as data from meteoritic samples and comets (see, e.g., Öberg & Bergin 2021; Öberg *et al.* 2023, and references therein). Eventually, the envelope will be fully dispersed, and the disk—now referred to as protoplantary disk—will be actively undergoing planet formation. Ice processes, such as diffusion, chemistry, and sublimation, will continue to shape the chemical composition and structure of these disks. They will determine which species, and in what physical state, will be incorporated into forming planets and planetesimals. For instance, the locations at which volatiles transition from ice to gas, known as snowlines, play an important part in determining planetary composition. Within them, molecules exist as gases, and might contribute to planet atmospheres. Beyond them, they remain solid and may be incorporated into planetesimal cores. Snowlines, particularly of hydrogen sulfide (H_2S), are a central topic of Chapter 5.

1.3.3 The missing sulfur problem

A significant portion of this thesis focuses on the formation and destruction of sulfur-bearing ice molecules. Interstellar sulfur has been a long-standing topic of discussion in the astrochemical community due to its conspicuously low detectable abundances compared to cosmic values—a discrepancy known as the "missing sulfur problem". While identifying potential reservoirs for this missing sulfur is not a central focus of this thesis, it is closely related to the topics explored in Chapters 4, 5, 6, 7, and 8. Therefore, it is relevant to briefly summarize the current state of this discussion here.

Among the over 320 molecules detected in the interstellar medium to date, at least 30 contain one or more sulfur atoms (McGuire 2022). Sulfur is one of the most common elements in space (S/H$\sim$1.35$\times$10^{-5}; Asplund *et al.* 2009), and S-bearing species are observed in the gas phase throughout most stages of star and planet formation: in clouds (e.g., Drdla *et al.* 1989; Agúndez *et al.* 2025), protostars (e.g., Blake *et al.* 1987; Drozdovskaya *et al.* 2018), and protoplanetary disks (e.g., Fuente *et al.* 2010; Rivière-Marichalar *et al.* 2021; Le Gal *et al.* 2021), as well as in Solar System bodies such as comets (e.g., Calmonte *et al.* 2016; Altwegg *et al.* 2022), and satellites (e.g., Moullet *et al.* 2008; Cartwright *et al.* 2020). Extragalactic sulfur-bearing species have also been detected (e.g., Martín *et al.* 2003, 2005). Identified molecules range in complexity, from simple diatomic species such as CS and SO to complex organics such as thioacetaldehyde (CH_3CHS), methanethiol (CH_3SH), and ethanethiol (CH_3CH_2SH) (e.g., Linke *et al.* 1979; Kolesniková *et al.* 2014; Agúndez *et al.* 2025). Note that the references provided here represent only a small subset of the broader literature, as numerous other studies have reported detections of sulfur-bearing molecules, from simple to complex, across a wide range of astrophysical environments.

In spite of this widespread detection, derived abundances in dense starless cores, protostars, and protoplanetary disks can only account for up to a few percent of the total expected cosmic value (e.g., Tieftrunk *et al.* 1994; Wakelam *et al.* 2004; Anderson *et al.* 2013; Vastel *et al.* 2018; Fuente *et al.* 2019; Le Gal *et al.* 2019; Rivière-Marichalar *et al.* 2019, 2020; Le Gal *et al.* 2021; Bouscasse *et al.* 2022; Fuente *et al.* 2023), with the bulk of the sulfur content remaining elusive. In diffuse clouds, however, sulfur is undepleted. One of the main hypothesis to explain the missing sulfur is that it is locked away in or underneath the ice mantles that shroud interstellar dust grains, in a state that is difficult to detect. H_2S could be a good candidate to explain the depletion of sulfur since it is efficiently formed on ices via the hydrogenation of S atoms (see, e.g., Garrod *et al.* 2007; Vidal *et al.* 2017). However, solid-phase interstellar H_2S has not been unequivocally detected yet, and only upper limits are available so far (e.g., Jiménez-Escobar & Muñoz Caro 2011a; McClure *et al.* 2023). These upper limits are not sufficient to account for the bulk of the missing sulfur, meaning that H_2S ice is likely undergoing effective solid-state destruction pathways that prevent it from accumulating onto dust grains (see, e.g., Garrod *et al.* 2007; Jiménez-Escobar & Muñoz Caro 2011a; Oba *et al.* 2018; Cazaux *et al.* 2022; as well as Santos *et al.* 2023b, 2024a,b—Chapters 4, 6, and 7 of this thesis—and references therein). Other proposed solid reservoirs are in the form of sulfur chains (e.g., S_n, H_2S_n; Wakelam *et al.* 2005; Calmonte *et al.* 2016; Shingledecker *et al.* 2020; Cazaux *et al.* 2022), sulfide minerals (e.g., FeS; Keller *et al.* 2002; Köhler *et al.* 2014; Kama *et al.* 2019), or even a combination of a wide range of simple organosulfur compounds hardly observable on their own (Laas & Caselli 2019). More recently, ammonium hydrosulfide salt (NH_4SH) has been invoked as a promising semirefractory sulfur reservoir candidate due to its high detected abundances in comet 67P/Churyumov-Gerasimenko (Altwegg *et al.* 2022) and tentatively in protostars, where it could account for up to 20% of the missing sulfur (Slavicinska *et al.* 2025). Although important advances surrounding the sulfur depletion problem have been achieved in the last decades, the state of the bulk of the interstellar sulfur content is ultimately still under debate. This distinctive characteristic unique to sulfur-bearing species makes them prominent puzzle pieces in understanding the evolution of volatile and refractory components throughout the different stages of star and planet formation, and particularly interesting cases for direct comparisons between interstellar ice and gas.

1.4 Laboratory astrochemistry

The field of astrochemistry is built upon three foundational pillars: observations, models, and experiments. Both observations and models fundamentally rely on laboratory experiments, alongside theoretical calculations, to derive meaningful interpretations of the phenomena under investigation (Cuppen *et al.* 2024). While calculations offer their own unique avenues of exploration that are certainly valuable the field, this thesis focuses on the laboratory component of experimental astrochemistry—whose indispensable role is briefly outlined here.

In the context of observations, laboratory-derived spectra of solid and gas-phase species are essential for identifying molecular features and interpreting telescope data (see, e.g., Boogert *et al.* 2015; Widicus Weaver 2019). While *ab initio* computational methods can help narrow down possible identifications for unknown spectral features, only laboratory measurements provide the level of precision required for definitive assignments. Similarly, determining column densities from observations depends on prior laboratory measurements of fundamental molecular properties. In the solid state, comprehensive measurements of infrared absorption band strengths across a range of relevant temperatures and ice mixing conditions are necessary for accurately quantifying ice abundances (e.g., Bouilloud *et al.* 2015). Additionally, laboratory measurements of optical constants for astrophysically-relevant solid media are necessary to properly model the scattering of light interacting with astronomical objects (e.g., Gerakines & Hudson 2020). In the gas phase, molecular excitation levels in interstellar environments often deviate from local thermodynamic equilibrium (LTE), where a single temperature characterizes the population distribution of rotational levels. In such cases, accurately determining column densities requires knowledge of collision rate coefficients to account for the interplay between collisional and radiative processes governing molecular excitation. While most collisional rate coefficients come from theory (e.g., van der Tak *et al.* 2020), laboratory experiments on selected transitions and systems are needed to benchmark the accuracy of calculated rate coefficients (Smith 2011).

Similarly, astrochemical models rely on key parameters, such as reaction rate coefficients and product branching ratios, which must be determined both for the solid and the gas phases. While theoretical predictions can provide useful estimates, in many instances these parameters must be determined experimentally. For example, gaseous neutral-neutral reaction rate coefficients often exhibit temperature dependencies that contradict theoretical predictions (Smith 2011). In the solid state, reactions rates and branching ratios are not the sole factors governing surface chemistry. Adsorption, desorption, and diffusion processes are also intertwined and collectively shape the chemical evolution of interstellar ices. These processes are difficult to fully constrain from first principles, making laboratory experiments essential for determining these convoluted parameters (Cuppen *et al.* 2017, 2024).

1.4.1 An overview of ice experiments

Much of this PhD thesis involves experiments on the chemical evolution of interstellar ices, which are performed using apparatuses designed to simulate the conditions typical of space environments. First, the common features of these setups, including the analytical techniques employed, are described. The specific details of each setup are then provided in the subsequent subsections. For better context, an example setup is shown in Figure 1.8, which was used for the largest fraction of the experimental works presented in this thesis (Chapters 2, 4, 6, and 7). In a nutshell, ice analogue experiments involve growing thin ($\sim 0.1-100$s monolayers, ML) ice films via freeze-out of gas onto a cold (typically $\sim 10-15$ K) substrate, and studying the physicochemical behavior of these ices under controlled conditions. To simulate as well as possible the low pressure conditions of interstellar space, experiments are performed under ultra-high vacuum (UHV; $\lesssim 10^{-9}$ mbar), achieved through dedicated vacuum pumping systems. At such pressures, the residual atmosphere consist mostly of H_2, with minimal water contamination (i.e., residual water deposition rates of $\lesssim 0.01$ ML/h). Interstellar temperature conditions are reproduced using cryogenic techniques. In all experimental setups used in this thesis, this is achieved with closed-cycle helium cryostats attached (either directly or via an interface) to the substrate. These systems allow a controlled manipulation of the substrate temperature using resistive heating wires. While the exact temperature ranges vary across the different setups used here, and even over time within the same setup, the typical range explored in this thesis remains within $\sim$ 10–300 K. The physicochemical processes of interest can then be induced by a variety of triggers. This thesis primarily focuses on atom- and radical-induced reactions, particularly those initiated by thermalized atomic hydrogen interacting with the other ice constituents (Chapters 2, 4, 6, and 7). Additionally, heat-driven processes are explored in Chapter 5, while ice processing induced by infrared radiation is examined in Chapter 3.

Ices can be grown sequentially to form distinct layers or concomitantly to produce ice mixtures. Furthermore, experimental deposition conditions can be categorized into two types: predeposition and codeposition, each serving a distinct purpose in terms of phenomena being probed. In predeposition, a species or mixture is first deposited onto the cold substrate and subsequently exposed to a trigger. This method allows for the changes in the ice to be monitored as a function of time, or of trigger fluence, enabling the determination of kinetic properties by fitting the time-resolved data with rate equations. For instance, this approach was used in Chapter 4 to investigate the product formation and the non-thermal sublimation kinetics of H_2S ice exposed to H atoms. However, a key limitation of the predeposition method is that it is restricted by the penetration depth of the trigger, which is typically just one or two monolayers for atomic hydrogen. As a result, this method is less suited for studying low-yield processes, for instance when the goal is to investigate multi-step reaction pathways. In codeposition, by contrast, the ice is grown on the substrate while simultaneously being exposed to the trigger. The continuous supply of reactants enables a steady formation of reaction products proportional to the duration of the deposition, facilitating their production above instrumental detection limits. Additionally, by controlling the relative deposition rates of different reactants and monitoring their impact on product yields, it is possible not only to optimize experimental conditions for better data interpretation but also to infer details about the underlying chemical networks. This strategy was employed, for instance, in Chapters 2, 6, and 7 to investigate how variations in atomic hydrogen abundance influence the equilibrium of product yields.

In terms of analytical techniques, this thesis primarily employs infrared spectroscopy and mass spectrometry. The former is used to monitor the ice composition and abundance *in situ*, and in all cases for this thesis, is performed using a Fourier-transform infrared spectrometer (FTIR) combined with a mercury cadmium telluride

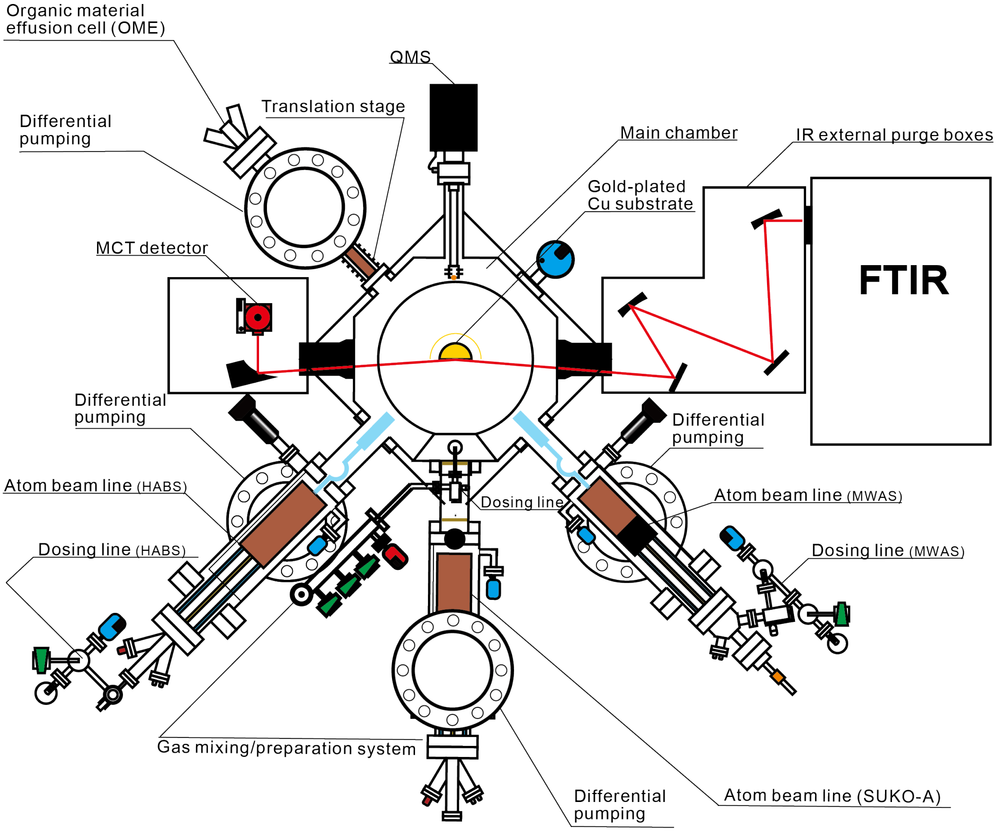

Figure 1.8: Top-view schematic of SURFRESIDE^3 in the configuration used for this thesis. Adapted from the earlier versions shown in Ioppolo *et al.* (2013) and Chuang (2018).

(MCT) detector cooled by liquid nitrogen. The FTIR emits infrared light, typically covering the range of 4000–700 cm^{-1} with a resolution of 1 cm^{-1}[6], which then either reflects off the substrate (when in reflection mode) or passes through it (when in transmission mode) before reaching the detector. More information on these two modes are presented in Sections 1.4.2 and 1.4.4, as they depend on the setup geometry and the choice of substrate material. Ice films grown on top of the substrate may interact with infrared radiation, producing absorption features in the spectra if they are infrared active. For a molecular vibration to be infrared active, it must induce a change in the dipole moment function (i.e., $\mathrm{d}\mu/\mathrm{d}Q \neq 0$, where μ is the dipole moment and Q is the vibrational coordinate), and the intensity of the absorption feature will be proportional to $(\mathrm{d}\mu/\mathrm{d}Q)^2$. Homonuclear diatomic species, for instance, have $\mathrm{d}\mu/\mathrm{d}Q = 0$ and therefore lack electric-dipole allowed infrared transitions, thus their infrared transitions are typically not detectable via conventional IR spectroscopy[7].

Infrared features in the solid state are often broad as a result of the range of molec-

---

[6] While higher resolution (0.5 cm^{-1}) is possible, it was not required for the scientific goals of this thesis.

[7] One notable exception is H_2, which due to its high abundance, is detectable by infrared observatories in astrophysical environments through its weak second-order electric quadrupole transitions.

ular interactions that produce variations in vibrational mode strengths. This effect is especially pronounced in amorphous solids, which exhibit a higher degree of structural disorder. The chemical environment of a species—such as its mixing conditions and the nature of the surrounding molecules—also strongly influences the shape of its infrared bands. Solid-state IR features are thus typically highly degenerate, especially for molecules with similar functional groups. As a result, laboratory assignments based solely on infrared spectroscopy performed at $\sim$10 K can be challenging, particularly for complex ice mixtures containing structurally similar molecules. One approach to produce an assignment is to compare the relative intensities of different absorption features that are thought to originate from the same molecule in the ice, as these tend to be less degenerate across different species. However, this method remains difficult in complex mixtures, where absorption features blend and it is not trivial to isolate individual contributions to the overall feature intensity. Isotope-labeled control experiments provide another strategy to mitigate these issues. Changes in a molecule's reduced mass, particularly for the moieties directly involved in a given vibrational transition, alter vibrational strengths and thus shift its frequencies. Heavier isotopologues exhibit a redshift in their infrared spectrum, which can help confirm spectral assignments in the laboratory. Additionally, differences in the volatilities of ice species can also be leveraged for spectral identification, provided that the molecules are not fully entrapped in less-volatile matrices. This can be achieved through temperature-programmed desorption (TPD) experiments, where the substrate is gradually heated at a constant rate. As the ice film reaches the sublimation temperatures of its components, they desorb, and the disappearance of absorption features at specific temperatures can provide information about the sublimation temperature of its carriers. This approach also allows for the isolation of spectral features from less volatile constituents within an ice mixture through a distillation-like process: as the ice film reaches the sublimation temperatures of the more volatile components, they sublimate first, leaving behind the less volatile species that can then be assigned via their infrared features (see Figure 1.9 for an example of distillation-facilitated assignment).

The integrated absorbance of an infrared feature ($\int Abs(\nu)\mathrm{d}(\nu)$) can be used to determine the column density of its carrier species via a modified Beer-Lambert law (see, e.g., Bouilloud *et al.* 2015 for a derivation of this relation):

$$N_X = \ln 10 \frac{\int Abs(\nu)\mathrm{d}(\nu)}{A_X}, \tag{1.2}$$

where N_X is the species' column density in molecules cm^{-2} and A_X is its absorption band strength in cm molecule^{-1}. The $\ln 10$ factor is employed to convert the integrated absorbance to optical depth scales. As discussed previously, band strength values are influenced by factors such as the ice mixing environment and ice morphology. Additionally, in setups utilizing reflection mode, the band strength is further affected by the optical properties of the infrared beam, which depend on the system's optical geometry. This introduces setup-dependent variations in the band strength, so literature values measured in transmission mode should not be directly applied to reflection-mode experiments. Instead, band strength measurements should be performed under the same experimental conditions, or a reflection-to-transmission conversion factor must be determined for the setup. These considerations will be addressed further in Section 1.4.2, which discusses a setup operating in reflection mode.

The other analytical tool employed throughout this thesis is mass spectrometry,

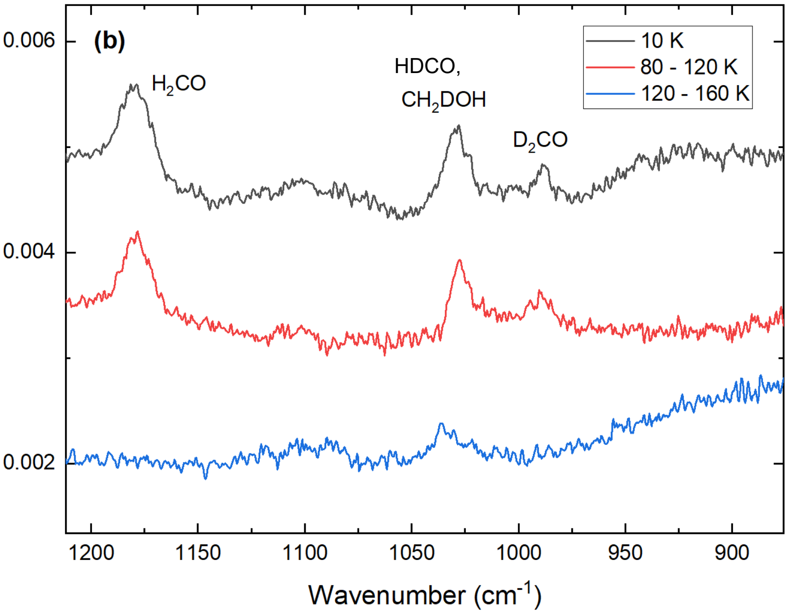

Figure 1.9: Infrared spectra measured during a TPD experiment. At 10 K, the absorption feature of CH_2DOH cannot be unambiguously identified due to blending with a HDCO feature. However, after formaldehyde fully desorbs (below 120 K), the absorption feature of the less volatile CH_2DOH becomes isolated. Figure from Chapter 2 (Santos *et al.* 2022b).

specifically using quadrupole mass spectrometers (QMS). In these instruments, gaseous species in the chamber are ionized via 70 eV electron impact from electrons generated by a hot filament at the tip of the QMS. While other electron energies are allowed, 70 eV is the stardard and the only value used here. The resulting ionized species are guided to the quadrupole mass filter, which selects for ions with specific mass-to-charge (m/z) ratios based on preset parameters. The filter consists of four parallel cylindrical rods, with each opposing rod pair electrically connected. An RF voltage with a DC offset is applied between the pairs of rods, allowing only ions with a particular m/z ratio to maintain a stable trajectory and reach the detector, while others develop unstable trajectories and collide with the rods.

Quadrupole mass spectrometers are powerful tools for molecular identification of desorbed ices. For instance, during a TPD experiment, when the substrate temperature reaches the sublimation range for a given molecule (provided it is not trapped in a less volatile ice matrix), it transitions into the gas phase and may be detected by the QMS. Upon electron impact ionization at 70 eV, molecules fragment into characteristic, energy-dependent patterns that serve as molecular fingerprints. Databases such as NIST[8] provide extensive mass fragmentation patterns for 70 eV electron bombardment, which can be used as reference standards to identify molecules desorbing from the ice at specific temperatures. This approach can be further strengthened by correlating QMS detections with the simultaneous disappearance of infrared features, providing robust assignments of ice species. Additionally, QMS measurements are

---

[8] https://webbook.nist.gov/chemistry/

typically at least an order of magnitude more sensitive than infrared spectroscopy of ice analogues, enabling the detection of less abundant reaction products.

Beyond serving as an assignment tool, the QMS can also be used as a quantification method under the high pumping speeds typical of UHV chambers. The integrated ion current from the mass fragments m/z of a species desorbing during a TPD experiment is related to the column density of that species by (Martín-Doménech *et al.* 2015):

$$N_X = k_{\mathrm{QMS}} \frac{a(m/z)}{\sigma_X^+ \cdot I_F(z) \cdot F_F(m) \cdot S(m/z)}, \tag{1.3}$$

where N_X is the total column density of desorbed species X, k_{QMS} is a proportionality constant, $a(m/z)$ is the integrated area of the desorption peak corresponding to a given mass fragment m/z from species X, σ_X^+ is the molecule's first ionization cross section at 70 eV, $I_F(z)$ is the fraction of ionized molecules with charge z, $F_F(m)$ is the fraction of molecules leading to a fragment of mass m, and $S(m/z)$ is the QMS sensitivity to the mass fragment of interest. For most molecules studied in this thesis, the ionization cross section σ_X^+ is either available in the literature or can be inferred from other molecular properties (see, e.g., Chapter 7). Under the experimental conditions explored here, only singly-charged mass fragments are relevant, so $I_F(z) = 1$. $F_(m)$ can be derived if the fragmentation pattern of the molecule is known, while $S(m/z)$ must be measured for a given mass spectrometer under a specific setup configuration. The proportionality constant, k_{QMS}, depends on the fraction of desorbed molecules that can reach the QMS and is thus a setup-dependent value that must be calibrated in order to derive absolute column density measurements. To determine relative abundances, Equation 1.3 for species X can be divided by the same equation for species Y. Assuming analogous pumping speeds for both molecules X and Y (a reasonable assumption, see e.g. Martín-Doménech *et al.* 2015), the k_{QMS} constant cancels out, enabling relative abundances to be determined without it.

The desorption rate of a given species as a function of temperature, measured by the QMS in units of current per Kelvin during TPD, can also be used to derive the species' sublimation parameters—such as its binding energies and desorption attempt frequencies under specific coverage regimes and substrate condition (e.g., Minissale *et al.* 2022). Coverage regimes can be broadly categorized into two cases: the multilayer regime, where desorption follows zeroth-order kinetics due to a constant number of adsorbates available for desorption at any given time, and the submonolayer regime, where the varying number of adsorbates results in first-order kinetics. In the former, binding energies are primarily dictated by intermolecular interactions between adsorbates of the same kind, whereas in the latter, they are dominated by interactions between the adsorbate and the substrate. This analysis is explored in detail in Chapter 5, where sublimation parameters and the corresponding snowline positions of H_2S in protoplanetary disk midplanes are determined. Furthermore, non-thermal desorption processes can also be studied by analyzing the QMS signal of a molecule's mass fragment—proportional to its desorption rate—as a function of trigger fluence. This is done in Chapter 4, where the kinetics of the non-thermal desorption of H_2S due to its excess heat of formation are explored using both infrared spectroscopy and mass spectrometry. Although QMS analyses have some limitations, the most notable being the destruction of the sample, they remain a powerful and versatile tool in astrochemical research.

1.4.2 SURFRESIDE^3

Chapters 2, 4, 6, and 7 of this thesis present work conducted using the SURFRESIDE^3[9] experimental setup, located at the Laboratory for Astrophysics at Leiden University, the Netherlands. This setup is specifically designed to investigate atom- and radical-induced reactions in interstellar ice analogues and is described in detail by Ioppolo *et al.* (2013) and Qasim *et al.* (2020b). A top-view schematic of the current system is shown in Figure 1.8.

The base pressure in the main chamber is of $\sim 10^{-9}$ mbar at room temperature and $\sim 10^{-10}$ mbar at 10 K. At its center, a gold-plated copper substrate is mounted on the tip of a closed-cycle helium cryostat (CH-204 SF; compressor HC-4E1). The substrate temperature can be controlled between $\sim 9 - 450$ K using resistive heating wires, and is monitored by two silicon diode sensors with an absolute accuracy of 0.5 K. The setup includes three atom source chambers and an organic material effusion cell chamber, each differentially pumped to UHV pressures. These chambers are connected to the main chamber with UHV shutter valves and/or gate valves. Additionally, a high vacuum ($\lesssim 10^{-5}$ mbar) manifold is used to prepare and introduce vapors and gases into the main chamber. Vapors from liquid or solid samples are admitted into the manifold through an ultratorr connection, while gases enter via swagelock valves. The admitted species can then be stored in two separate dosing line reservoirs, and then be inlet into the main chamber through two capillary tubes controlled by two high-precision leak valves that enable ice deposition with submonolayer precision.

The hydrogen atom beam source (HABS; Dr. Eberl MBE-Komponenten GmbH; Tschersich 2000) produces atomic hydrogen or deuterium via thermal cracking of H_2 or D_2 molecules using a tungsten filament. The molecular gas is admitted into a dedicated dosing line, then introduced into the HABS chamber by a leak valve. The chamber pressure is adjusted to control the atomic flux reaching the substrate, typically on the order of 10^{12} atoms cm^{-2} s^{-1}. The microwave atom source (MWAS, Oxford Scientific Ltd; Anton *et al.* 2000) operates by generating free electrons with sufficient kinetic energy to break apart and ionize molecules, creating a plasma. Consequently, it can be used to generate atomic species such as O and N, as well as radicals such as OH, depending on the gases inlet into the MWAS chamber. It is powered by a 2.45 GHz microwave power supply (Sairem) delivering up to 200 W, coupled into a microwave cavity. An ion trap deflects ions to prevent them from entering the main chamber. Like HABS, gases are admitted into the MWAS chamber via a dedicated dosing line controlled by a leak valve, with attainable atom/radical fluxes also around 10^{12} atoms cm^{-2} s^{-1}. In the case of H or D atoms, both HABS and MWAS can be used simultaneously to maximize the atom flux, as is done in Chapter 2. On the exit path of both the HABS and the MWAS, nose-shaped quartz pipes are placed to cool the species through multiple collisions with their walls. This allows the species to quench and thermalize before reaching the substrate, and also shields the substrate from any UV light produced by the MWAS plasma. The carbon atom source (SUKO-A, Dr. Eberl MBE-Komponenten GmbH; Krasnokutski & Huisken 2014) generates ground state C($^3P_0$) atoms by resistively heating a tantalum filament packet with graphite powder. This design is advantageous because it predominantly produces atomic carbon, unlike conventional carbon rod heating methods that generate clusters. A dosing line is not required, but filaments must be replaced after $\sim 10 - 15$ hours

---

[9] SURFace REaction SImulation DEvice^3

of operation under standard conditions. Finally, the organic material effusion cell (OME Dr. Eberl MBE-Komponenten GmbH) allows the deposition of high-vapor-pressure organic materials such as sugars and aminoacids by heating a conical quartz crucible containing the sample at temperatures up to 300 °C. The source is mounted on a 10-inch linear translator (Hositrad HOBLT27S-10), allowing precise positioning near the substrate during deposition. Like for SUKO-A, the OME does not require a dosing line. All three atomic sources, as well as the effusion cell, are equipped with water-cooled shrouds to prevent overheating.

SURFRESIDE^3 features two analytical tools: an FTIR spectrometer (Agilent Cary 640/660) with a liquid-nitrogen-cooled MCT detector and a QMS (Hidden Analytical 3F RGA). The IR pathway is purged of atmospheric H_2O and CO_2 using filtered compressed air. In this setup, IR light is emitted from the FTIR and focused by external optics onto the sample, where it reflects off the gold-plated substrate before being collected by the MCT detector. It thus operates in reflection mode, also known as Reflection Absorption Infrared Spectroscopy (RAIRS). RAIRS is chosen over transmission spectroscopy because of its higher sensitivity: the IR path passes through the ice twice—upon incidence and reflection—and the p-polarized electric field intensity of the IR light is enhanced due to the shallow grazing angle ($\sim$ 10° to the surface place) on the gold substrate (see the discussion in Qasim 2020). However, the shape and relative intensities of absorption features in RAIRS spectra can vary significantly depending on experimental conditions (e.g., ice thickness, IR path geometry, and the instrument setup), making them unsuitable for direct comparison with observational infrared data, which is acquired in transmission mode (see, e.g., Rocha *et al.* 2022). Moreover, band strength values measured in transmission mode cannot be directly applied to SURFRESIDE^3 experiments. To address this, the band strengths of H_2S—the most frequently used species in this thesis—and CO were experimentally determined for this setup. This was done by depositing ice at a constant rate while simultaneously measuring its thickness via laser interference (using a HeNe laser) and recording its absorption spectra with RAIRS. The detailed procedure for H_2S is discussed in Chapter 4, and is repeated with CO. Their resulting estimated band strengths are: A_{CO}(C-O str.) = $(4.2\pm0.3)\times10^{-17}$ cm molecule^{-1} and $A_{\mathrm{H_2S}}$ (S-H str.) = $(4.7\pm0.1)\times10^{-17}$ cm molecule^{-1}. From these values, a mean reflection-to-transmission conversion factor of ~ 3.2 is derived based on their corresponding transmission band strengths (Bouilloud *et al.* 2015; Yarnall & Hudson 2022). Setup-dependent calibrations of the QMS sensitivity are also necessary. Here, we adopt the calibration values provided by Chuang (2018) for the same experimental setup.

1.4.3 LISA

The work presented in Chapter 3 was conducted using the LISA[10] experimental setup located at the HFML-FELIX Laboratory, Radboud University, the Netherlands. The setup has been rebuilt multiple times in recent years, and details on the version used in this thesis can be found in Ioppolo *et al.* (2022). It consists of an UHV end station coupled to the tunable, high-power, short-pulsed radiation from the free-electron lasers (FEL) at the HFML-FELIX: FELIX-1 ($\sim 30-150$ μm), and FELIX-2 ($\sim 3-45$ μm). The main chamber operates at a base pressure of $\sim10^{-9}$ mbar at room temperature, at the center of which a gold-plated copper substrate is in thermal contact with a

---

[10] Laboratory Ice Surface Astrophysics

closed-cycle helium cryostat head (Sumitomo, CH-204SB) supported by a compressor (HC-4E). The substrate temperature can be controlled between $\sim 20 - 300$ K via resistive heating, and is measured by a silicon diode. Pure gas and vapors, as well as mixtures, are prepared in a manifold with a base pressure of 10^{-4} mbar and admitted into the main chamber through a dosing line controlled by an all-metal leak valve. The substrate position can be adjusted vertically using a z-translation stage with a 2-inch stroke, allowing for different spots in the ice to be probed during experiments.

The LISA end station is coupled to the FEL beamline so that the beam path reaches the substrate. Three gate valves are installed in series along the FEL beam path before it enters the main chamber. The first two contain CsI and TPX windows, which are transparent in the IR and THz ranges, respectively. Their intent is to optimize switching between FELIX-1 and FELIX-2 during a shift (8 hours). The third gate valve is a blank, used to block the FEL beam when irradiation is not required. For analytical techniques, LISA is equipped with an FTIR spectrometer (VERTEX 80v, Bruker) coupled to a liquid-nitrogen-cooled MCT detector for infrared spectra acquisition in reflection mode. A QMS (MKS Instruments) is also positioned facing the gold substrate for analysis of the gas phase.

1.4.4 SPACE-KITTEN

The experimental setup SPACE-KITTEN[11], located at the Öberg Astrochemistry Lab at the Center for Astrophysics, Harvard University, was used in Chapter 5 of this thesis. This setup is dedicated to studying thermal processes in interstellar ice analogues and is described in detail elsewhere (Simon *et al.* 2019, 2023). It consists of a UHV chamber with a base pressure of $\sim 10^{-9}$ Torr at room temperature. At the center of the chamber, a CsI window is mounted on an optical ring sample holder attached to a closed-cycle helium cryostat (Advanced Research Systems model DE204S). To minimize vibration transfer from the cryocooler to the CsI window, the cryostat is integrated with a DMX-20B interface that uses helium exchange gas to decouple the window from the cold tip. The substrate temperature is controlled via resistive heating over a range of $12 - 350$ K, with a precision of ± 0.1 K and an absolute accuracy of ~ 2 K, monitored by silicon diode sensors. Gas and vapor samples are prepared in a manifold maintained at base pressures of $< 5 \times 10^{-4}$ Torr before deposition. After preparation, species are introduced into the main chamber via a stainless steel tube doser (4.8 mm diameter) positioned 2 inches from the substrate. The doser is connected to the manifold through a variable leak valve and is mounted on a compact z-translation stage (MDC Vacuum Products, LLC), allowing to approach the doser to the substrate during deposition.

SPACE-KITTEN is equipped with an FTIR spectrometer (Bruker Vertex 70) with a liquid-nitrogen-cooled MCT detector operating in transmission mode. The UHV chamber is housed within the FTIR's sample compartment, with the IR optical path aligned with the horizontal axis of the chamber. The chamber and the FTIR are interfaced on each side with two IR transparent KBr windows that are differentially pumped, as well as with vibrational damping mounts. The optical path of the IR is purged with pure, dry nitrogen gas to prevent atmospheric interference. Additionally, the setup includes a QMS (QMG 220M2, PrismaPlus Compact) positioned near the sample holder. For the scientific objectives of Chapter 5, it was not necessary to

---

[11] Surface Processing Apparatus for Chemical Experimentation–Kinetics of Ice Transformation in Thermal ENvironments

determine the sensitivity of the QMS as a function of m/z.

1.5 Observational astrochemistry

Telescopes offer another fundamental avenue for astrochemical research, providing the only means to obtain direct empirical evidence of the chemistry in star- and planet-forming regions beyond our Solar System. Throughout this thesis, observations of interstellar ices and gas serve to contextualize and motivate the investigations presented in each chapters. Additionally, in Chapters 8 and 9, we utilize radio telescopes to observe emission lines from the rotational transitions of relevant molecules, which provide insights into their chemical evolution and origins.

1.5.1 Submilimeter and millimeter observations

Observations at submillimeter and millimeter wavelengths have led to the detection of the vast majority of interstellar molecules (McGuire 2022). This is largely because of the low energies associated with the levels whose transitions fall on such large wavelengths, which are more easily populated compared to higher-energy transitions. The primary type of molecular transition probed in these wavelengths are rotational lines, often in the ground vibrational state ($\nu = 0$)—though, in some instances, vibrationally-excited pure rotational lines are also observed. When sufficient energy is available to populate a molecule's rotational levels above the background radiation field, emission lines are observable. This occurs in warm regions such as hot cores, which are known for their rich spectra with forests of molecular emission lines (e.g., Belloche *et al.* 2013; Jørgensen *et al.* 2020), but emission lines are also observable even in much colder environments like dark clouds (e.g., Kaifu *et al.* 2004). In extremely cold environments where there is not enough energy to populate rotational energy levels, molecules can still be observed in absorption against the background continuum (e.g., Neufeld *et al.* 2012; Gerin *et al.* 2016). As a result, molecules can be observed in millimeter and submillimeter wavelengths across virtually all types of interstellar regions.

To observed these lines, millimeter-wave telescopes are employed. These instruments use antennas, typically consisting of paraboloid reflectors that focus incoming radiation onto a receiver. They can operate as either single-dish telescopes, which use a single antenna, or as interferometric arrays of antennas. In an interferometric array, multiple antennas are combined to form a synthesized aperture with an effective diameter much larger than that of an individual antenna. The separation between antennas, combined with Earth's rotation, introduces differences in the path length of incoming light from the observed source. These path length variations produce interference patterns that can be reconstructed into an image of the observed source (Thompson *et al.* 2017). Spatial resolution is inversely proportional to the effective antenna diameter, so interferometry is a powerful technique for achieving high spatial resolution by synthesizing an aperture much larger than would be possible with a single dish antenna. For instance, in its most extended configuration, the Atacama Large Millimeter/submillimeter Array (ALMA) can space its antennas up to ∼16 km apart, yielding spatial resolutions on the order of tens of milliarcseconds. However, because the gaps between antennas do not collect radiation, interferometers gather less total light than a single dish of equivalent size. Additionally, the sensitivity of an interferometer depends on the signal received by each individual antenna. As a result, even if the total collecting area of an array exceeds that of a single-dish telescope, its sensitivity may be lower if the individual antennas are too small. Nonetheless, other factors, such as receiver noise, also play a role in determining sensitivity. Ultimately, both single-dish and interferometric telescopes offer distinct advantages and limitations, and this thesis employs both techniques to study molecular emission lines toward massive young stellar objects.

1.5.1.1 ALMA

ALMA is an interferometer comprising 66 antennas located in the Atacama Desert in northern Chile. It includes 54 antennas with individual diameters of 12 m, which can be arranged in various configurations to achieve angular resolutions ranging from $\sim$0.01″to $\sim$9″. Large-scale observations are also possible using ALMA's compact configuration, which employs its 12 7-m dishes. ALMA operates over a broad frequency range of $\sim$35−950 GHz, with spectral resolution as high as $\sim$0.03 MHz (corresponding to $\sim$0.26−0.01 km s^{-1}, depending on frequency). This coverage is achieved using 10 different receivers, known as bands, each designed to capture a specific frequency range. In Chapter 8 of this thesis, publicly available ALMA Band 6 observations ($\sim$1.1−1.4 mm, or $\sim$211−275 GHz) with spatial resolutions of 0.5−1.5″and spectral resolutions of $\sim$0.5 MHz ($\sim$0.7 km s^{-1}) are used to investigate the abundances of key sulfur-bearing molecules in the inner envelopes of 26 massive young stellar objects.

1.5.1.2 APEX

The Atacama Pathfinder Experiment (APEX) is a 12-m single-dish telescope based on an ALMA prototype antenna, and like ALMA is also located in the Atacama desert in northern Chile. APEX currently operates over a spectral range of 157−850 GHz, with spatial resolutions between 6″to 39″, depending on the instrument. In Chapter 9, APEX observations with the Swedish-ESO PI Instrument (SEPIA180; Belitsky *et al.* 2018) alongside the Swedish Heterodyne Facility Instrument (SHeFI, decommissioned; Vassilev *et al.* 2008a) are used to conduct a spectral survey of methyl acetylene (CH_3CCH) towards the hot molecular core system G331.512-0.103 (R.A., decl. [J2000] = $16^{\rm h}12^{\rm m}10.^{\rm s}1$, $-51°28'38.''1$). We observe nine frequency setups within 170−205 GHz and 222−307 GHz, respectively, with spectral resolution of 0.06−0.13 km s^{-1} and spatial resolution of $\sim$17−39″.

1.5.2 Infrared observations

In emission, molecules can also be observed through their vibrational transitions, which typically occur at infrared wavelengths, provided sufficient energy is available to populate these excited levels. This is the case, for instance, in inner disk regions, where high gas densities and temperatures allow the detection of molecular emission lines from rovibrational transitions (e.g., Salyk *et al.* 2011). Other mechanisms, such as radiative pumping from a strong radiation field, can also help populate these energy levels (e.g., van Gelder *et al.* 2024). In the absence of such mechanisms, vibrational transitions can still be observed in absorption if a background radiation source is present and the environment is optically thin enough to allow some light to pass through and reach the telescope.

For the purpose of this thesis, infrared observations of interstellar ices are particularly interesting. Since molecules in the solid state lack the degrees of freedom necessary for rotational transitions, their vibrational modes provide the only direct means of observing ices. These observations typically occur in absorption, as the energy required for emission would generally lead to desorption of the molecules. The exceptions are torsion and lattice modes ($\sim$25−300 μm), which have excitation energies below the ice binding energies and thus might be observed in emission (Boogert *et al.* 2015).

Following the first observation of the 3.1 μm feature associated with H_2O ice towards the Orion BN/KL region (Gillett & Forrest 1973), numerous ice features have been identified, with profiles that reflect the complexities of their composition, mixing conditions, thermal history, and grain shape effects (Boogert *et al.* 2015). Such observations can be carried out using ground-based, airborne, or space telescopes. While ground-based telescopes were responsible for much of the early infrared investigations of the universe, and continue to offer powerful insights into interstellar ice composition (e.g., Boogert *et al.* 2022), they are inherently limited by light absorption and distortion caused by Earth's atmosphere. In contrast, airborne and space-based telescopes either mitigate or bypass these issues entirely, and have thus been instrumental in study of interstellar ices. The Kuiper Airborne Observatory (KAO; Haas *et al.* 1995) was a pioneering tool in this regard, allowing observations to be performed from above almost all of the water vapor in the Earth's atmosphere and thus providing unprecedented insights on the composition of ices (e.g., Willner *et al.* 1982). The subsequent launch of the Infrared Space Observatory (ISO), particularly through its short wavelength spectrometer (SWS), opened up the full mid-infrared spectrum to observations, offering the first comprehensive inventory of major interstellar ice features and providing the first glimpse of these ices in low-mass sources (van Dishoeck 2004). With the advent of the James Webb Space Telescope (JWST), the field has entered a new golden age, with observations confirming ice species that were previously undetected or only tentatively identified—including a range of complex organic molecules (Rocha *et al.* 2024) as well as deuterated water ice (Slavicinska *et al.* 2024).

1.5.3 Fundamentals of radiative transfer

To extract information from observed spectra, it is necessary to accurately describe how light propagates through a medium before reaching the telescope. The variation of specific intensity along the light path (dI_ν/ds) is described by (Rybicki & Lightman 1985):

$$\frac{dI_\nu}{ds} = -\alpha_\nu I_\nu + j_\nu. \tag{1.4}$$

where ds is the distance traveled by the beam, α_ν is the absorption coefficient, defined as the product of the density n of absorbing particles times their absorption cross section σ_ν, and j_ν is the monochromatic emission coefficient. In other words, energy emission increases the beam intensity, while absorption of radiation reduces it. Equation 1.4, known as the radiative transfer equation, provides a framework for modeling light-matter interactions. It serves as the basis for methods used to derive physical properties from observed molecular absorption and emission in space.

When molecular excitation and de-excitation are primarily driven by collisions, as is typical in high-density environments, the system is said to be in local thermodynamic equilibrium (LTE). Under these conditions, the population of a molecule's energy levels follows a Boltzmann distribution characterized by a single excitation temperature, and the population of each level is given by (Goldsmith & Langer 1999):

$$N_u = \frac{N_{\text{tot}}}{Q(T_{\text{ex}})} g_u e^{-E_u/k_{\text{B}}T_{\text{ex}}} \tag{1.5}$$

where N_u is the molecule's column density in the upper energy level of a given transition, N_{tot} is the total column density of the species in question, $Q(T_{\text{ex}})$ is its partition function (i.e., the sum of the populations across all energy levels), g_u is the statistical weight of the upper energy level, and E_u is its energy. Thus, in LTE, the total molecular column density can be derived from the column density of any individual transition if the excitation temperature is known, and the excitation temperature corresponds to the kinetic temperature of the gas.

By solving the radiative transfer equation under LTE conditions, one can fit molecular emission lines with a Gaussian function to extract both the total column density and excitation temperature (see, e.g., Vastel 2014; Nazari 2024, for a more detailed explanation). However, if only a single transition from a given molecule is observed, excitation temperature and column density become degenerate, meaning one can only be determined by fixing the other. This is the case in Chapter 8, where excitation temperatures are set to an average value typical of hot cores to allow column density determination. If transitions are optically thick, part of the emission will not be accounted for, leading to an underestimation of the column density. Moreover, if the telescope beam size is much larger than the size of the source, the measured intensity will be reduced by beam dilution, also underestimating the column density. The latter effect is particularly relevant for single-dish observations, for which beam sizes are larger.

In this thesis, we use the CASSIS software (Vastel *et al.* 2015) to solve the radiative transfer equation under LTE assumptions and fit the observed molecular emission lines to extract column densities and, where applicable, excitation temperatures. An example of such fits is shown in Figure 1.10 (Nazari 2024). Additionally, assuming LTE, the natural logarithm of the column density per statistical weight of different molecular energy levels is linearly correlated with the level's energy above ground state over k_{B}, with the slope of this relation yielding the excitation temperature and the y-intercept yielding the total column density (Figure 1.11; Goldsmith & Langer 1999). These plots, known as population diagrams, are used in Chapter 9 to determine the temperature and column density of the CH_3CCH gas surrounding a massive protostar.

1.6 This thesis

1.6.1 Chapter summary

Once thought to be chemically barren, the interstellar medium is now known to host a large variety of chemical species. Many of these, including simple molecules like H_2, and especially more complex organic molecules, result from processes taking place on icy dust grains. This thesis combines experimental and observational approaches to explore the physicochemical transformation of interstellar ices throughout the stages of star and planet formation—from clouds, to protostars, to protoplanetary disks.

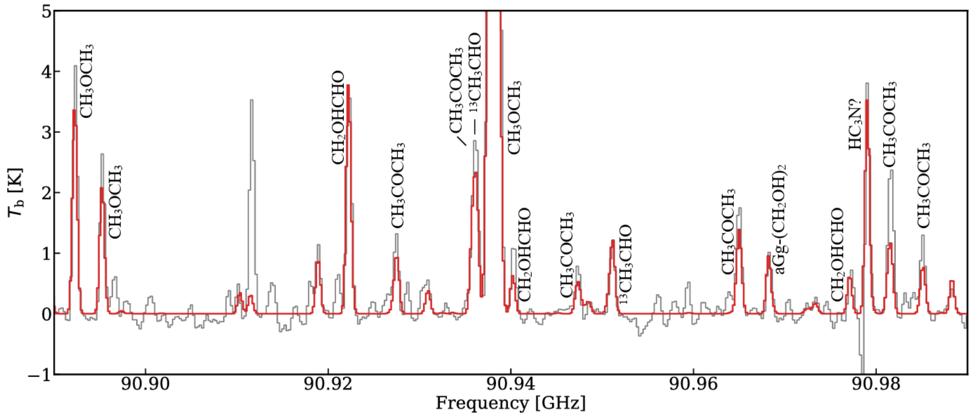

Figure 1.10: ALMA Band 3 observations towards IRAS 16293-2422 B (gray) superimposed by Gaussian fittings to a subset of the molecular emission lines (red). Figure from Nazari (2024).

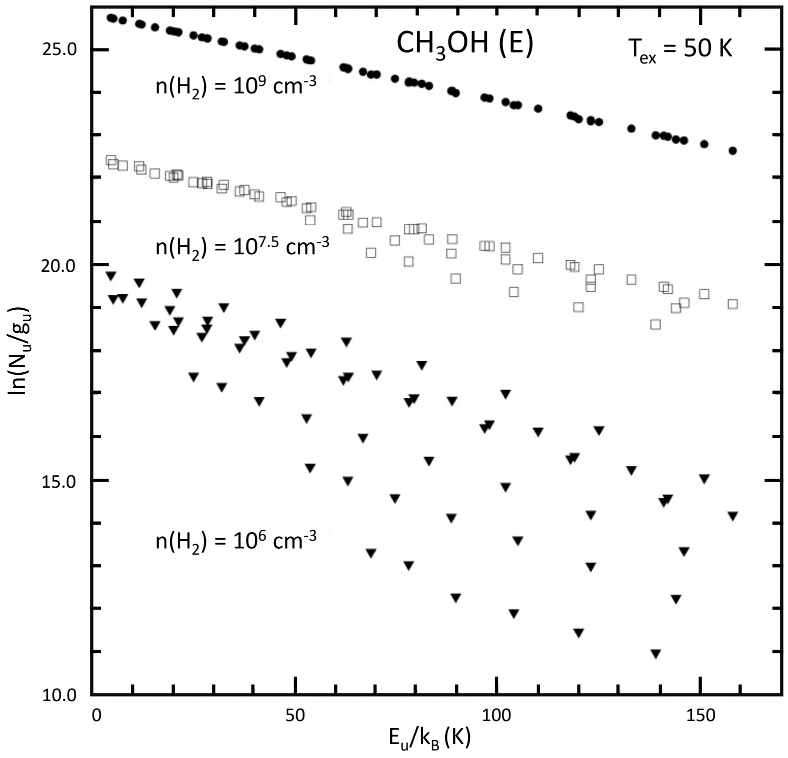

Figure 1.11: Population diagram of modeled optically thin CH_3OH rotational lines at varying hydrogen densities for $T_K = 50$ K. At low densities, sub-thermal excitation heavily affects the slope of the plot, particularly at high energies. For densities of 10^9 cm^{-3}, all modeled transitions are thermalized, and the data points follow a linear trend with no scattering. Figure adapted from Goldsmith & Langer (1999), see Figure 6 in Johnstone *et al.* (2003) for an alternative version.

The central question guiding this work is: *How do ice molecules form, transform, and desorb?*

To address this question, we explore how ices evolve under the influence of various phenomena throughout different stages of star and planet formation. We investigate the chemical networks that dominate in the cold environments of molecular clouds, where reactions are largely driven by "non-energetic" atom- and radical-induced processes. We also explore the stability of ices in these clouds, as well as potentially relevant non-thermal sublimation processes. Once gravitational collapse has begun, we turn to the thermal desorption of ices as they are heated by the protostar. We characterize sublimation front locations in disk midplanes, and leverage gas-phase observations of sublimated ices to gain insights into the chemical evolution and the physical properties of the sources. The main conclusions of each chapter are as follows:

On the formation and stability of O-bearing ices: the case of CO and CH_3OH

Chapter 2: Methanol (CH_3OH), a major component of interstellar ices and a key precursor of larger complex organic molecules, has long been thought to form through successive hydrogen addition to CO. However, recent kinetic Monte Carlo models have challenged this view, particularly regarding the final reaction step. Leveraging the kinetic isotope effect as a tool, we provide the first experimental confirmation that the reaction $CH_3O + H_2CO \rightarrow CH_3OH + HCO$ is the dominant final step to form methanol ice under laboratory conditions. The experimentally derived contributions from this pathway, along with the traditionally proposed hydrogen addition route ($CH_3O + H \rightarrow CH_3OH$), agree with kinetic Monte Carlo models under laboratory conditions. These models, when extended to molecular cloud conditions, confirm that this abstraction pathway dominates in the interstellar medium.

Chapter 3: Infrared photons from the interstellar radiation field can penetrate deep into molecular clouds, yet their interactions with ices remain largely unexplored experimentally. We utilize a free-electron laser large facility to irradiate pure CO and CH_3OH ices, as well as mixtures of the two, with near-monochromatic mid-infrared photons to explore the effects of resonant infrared irradiation on ice morphology. We find that ices undergo structural rearrangement as a result of on-resonance irradiation. In the cases of pure CO and ice mixtures, this rearrangement cannot be solely explained by thermal processing. We also find evidence for the loss of ice material, which we attribute to single-photon, non-thermal infrared-induced desorption mechanisms, particularly for indirect CO desorption resulting from resonant CH_3OH irradiation. Although this process is far less efficient than UV-induced desorption, its potential impact may be non-negligible due to the greater penetration depth of infrared photons in molecular clouds.

On sulfur-bearing ice chemistry and desorption

Chapter 4: H_2S ices are predicted to form very efficiently and were once considered strong candidates for the main interstellar sulfur reservoir in the solid state. However, its observed upper limits contradict this idea, suggesting that H_2S ice must undergo effective solid-state destruction mechanisms. To explore some of its most promising destruction pathways, we experimentally investigate the interaction of H_2S ice with thermalized hydrogen atoms. We show that HS radicals, formed *in situ* via the reaction $H_2S + H \rightarrow HS + H_2$, can initiate a sulfur-bearing chemical network, demonstrated here by the formation of H_2S_2 as a proof-of-concept. Additionally, we directly quantify the chemical desorption efficiency of H_2S formed via $HS + H \rightarrow H_2S$ by analyzing the gaseous signal recorded by the QMS. This direct approach is complemented by indirect measurements of the chemical desorption efficiency, derived from the loss of H_2S signal from the ice after accounting for H_2S_2 formation. The dominant destruction mechanism of H_2S ice under our experimental conditions is chemical desorption. However, as temperatures rise from 10 to 16 K, the formation of H_2S_2 becomes increasingly more significant, arguably due to enhanced diffusion.

Chapter 5: Although H_2S is unlikely to be the main sulfur reservoir in ices, there is still compelling evidence for its presence in non-negligible amounts ($\sim$1% relative to water). Understanding its desorption behavior is crucial for interpreting the sulfur chemical network and predicting in what physical state it may be incorporated by forming planets and planetesimals. For the first time, we experimentally characterize the sublimation dynamics of H_2S ice and derive its corresponding desorption temperatures and snowline positions in a representative T-Tauri disk midplane. We determine binding energies in the multilayer regime, where H_2S primarily interacts with other H_2S molecules, as well as in the submonolayer regime on top of a compact amorphous solid water substrate, that is, where H_2S interacts primarily with H_2O. Both cases lead to sublimation fronts located just interior to the CO_2 snowline. However, we find that the entrapment of H_2S in water ice is highly efficient ($\gtrsim$ 75%), effectively shifting its snowline position closer to the H_2O snowline, assuming it forms mixed with water. Therefore, H_2S is expected to remain in the solid phase throughout the entire region where comets and icy asteroids form.

Chapter 6: Building on the results of Chapter 4, we present compelling experimental evidence that HS radicals can efficiently react with CO and H in the solid state to form OCS ice. We propose a formation mechanism involving the HSCO complex: $HS+CO \rightarrow HSCO+H \rightarrow OCS+H_2$, similar to the formation of CO_2 ice. This reaction proceeds efficiently even under conditions of significant H_2S dilutions (5% with respect to CO) and low hydrogen abundances (H:CO=1.5:1). That, combined with the fact that HS radicals can be produced through both bottom-up ($S + H \rightarrow SH$) and top down ($H_2S + H \rightarrow SH + H_2$) pathways, makes this route a promising mechanism to forming OCS throughout various stages of cloud evolution.

Chapter 7: Further expanding on the ice sulfur network initiated by HS radicals, we find that its interaction with C_2H_2 and atomic H leads to the formation of a large number of species. We identify at least six sulfurated products: CH_3CH_2SH, CH_2CHSH, $HSCH_2CH_2SH$, H_2S_2, and tentatively CH_3CHS and CH_2CS. Experimental mixing ratios, as well as quantum chemical calculations, are employed to help pinpoint the underlying reactions driving this network. At higher H abundances, CH_3CH_2SH is preferentially formed due to a series of barrierless hydrogenation reactions leading to it—largely at the expense of other organic products. It thus acts as a sink in this chemical network.

Chapter 8: SO_2 and OCS are major volatile sulfur carriers and the only sulfur-bearing molecules detected in interstellar ices to date, making them the ideal candidates for directly comparing the volatile sulfur content in the gas and ices across star and planet formation. In this observational work, we derive the column densities of SO_2 and OCS towards the hot cores of 26 line-rich massive young stellar objects, observed as part of the ALMA Evolutionary study of High Mass Protocluster Formation in the Galaxy (ALMAGAL) survey. We derive their abundance with respect to methanol, which are compared among themselves and to gas-phase observations from low mass sources, as well as ice observations in clouds, protostars, and comets. For OCS, the abundances suggest ice formation during the high-density prestellar core stage, with minimal gas-phase reprocessing upon thermal sublimation in the hot core phase. It also appears to be largely inherited by comets. In contrast, SO_2 seems to also form in ices prior to star formation, but likely at earlier stages before the catastrophic CO freeze-out. It is more subject to gas-phase reprocessing upon sublimation and is only moderately inherited by comets.

On the physical conditions probed by gas-phase hydrocarbons: the case of CH_3CCH

Chapter 9: Methyl acetylene (CH_3CCH) is widely observed in star-forming regions and is known to be a reliable tracer of physical conditions such as density and temperature. It is thought to form from a combination of gas and solid-state processes. In this work, we conduct a spectral survey of the CH_3CCH gas towards the hot molecular core G331.512-0.103 using observations from the Atacama Pathfinder Experiment (APEX). By analyzing its temperature-sensitive spectral features, we derive the small-scale temperature distribution of the gas from single-dish observations. Based on the relative intensities of the $K = 2$ and $K = 3$ lines, we probe a temperature gradient in the gas ranging from $45 \lesssim T_{\rm ex} \lesssim 60$ K. The $K = 0$ transitions exhibit a distinct kinematic signature compared to the other lines in the K-ladders, suggesting they trace a different gas component. We hypothesize that this may correspond to a colder gas, as the spectra at low temperatures are dominated by low K-level lines.

1.6.2 Main conclusions and future directions

A significant portion of this thesis explores the formation of ice molecules under molecular cloud conditions, where temperatures are low ($\sim 10 - 20$ K) and chemistry is primarily driven by radical- and atom-induced reactions. The key reaction pathways identified in this work are summarized in Figure 1.12. Beyond these, the main takeaways of this thesis are outlined below, which also reveal some interesting new directions for future explorations:

1. The main formation mechanisms of interstellar ices may not always be the most intuitive ones (Chapter 2). As solid-state chemical networks depend on numerous convoluted effects whose final outcomes are challenging to predict, laboratory experiments that evaluate the contributions of different reaction pathways to interstellar ice complexity are essential. These can be achieved, for instance, by leveraging physicochemical principles such as the kinetic isotope effect.

2. While, over the past 20 years, significant progress has been made in understanding entrapment efficiencies for various matrix-volatile combinations, many open questions still remain regarding the underlying mechanisms governing volatile entrapment (Chapter 5). Elucidating these mechanism is crucial for accurately translating laboratory measurements to realistic disk conditions.

3. A prolific ice sulfur chemistry can be initiated by HS radicals, which form both via hydrogenation of S atoms in early cloud stages and via hydrogen abstraction

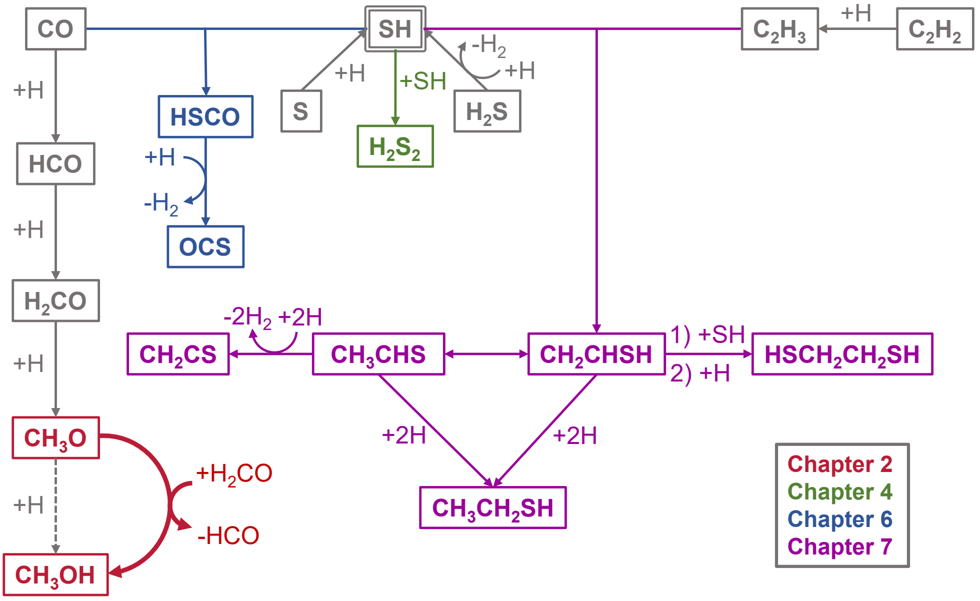

Figure 1.12: Summary of the new ice reaction pathways experimentally uncovered in this thesis.

from H_2S at later stages (Chapters 4, 6, 7). Solid-state reactions involving this radical offer a promising avenue for building a complex sulfur-bearing interstellar molecular inventory, and may also help explain why observationally-constrained H_2S ice upper limits are lower than expected based on its predicted formation efficiency.

4. The chemical environment of an icy molecule dictates the shape of its spectral signatures, available reaction partners, and desorption dynamics. It is thus paramount to understand not only *how*, but also *when* molecules are formed. Gas-phase observations of sublimated ices offer an interesting avenue to probing the formation history of less abundant species that are challenging to detect in ices. This approach reveals, for instance, that while both SO_2 and OCS predominantly form in ices during prestellar stages, SO_2 likely forms much earlier than OCS and/or is considerably more subject to post-sublimation reprocessing (Chapter 8).

5. The temperature-sensitive K-ladders of symmetric rotors, particularly those with different nuclear spin statistics (as is the case, e.g., for molecules with three equivalent hydrogen atoms like CH_3CCH), can be leveraged to infer the small-scale temperature gradients in the gas. This is particularly useful for single-dish observations, which lack the angular resolution to directly resolve these gradients (Chapter 9).

Overall, this thesis demonstrates how experiments and observations work in synergy to advance our understanding of the chemical evolution of volatiles in star- and planet-forming regions. This field is now experiencing a golden age, with state-of-the-art telescopes such as ALMA and JWST offering unprecedented sensitivity and resolution to probe both the gaseous and solid molecular inventory of interstellar space. By combining the capabilities of these telescopes, observations are now able to provide strong, direct empirical evidence for the interplay between gas and ice in these environments. Laboratory experiments are, arguably now more than ever, essential for accurately interpreting these observations. Furthermore, as experiments push the limits of *in-situ* detection of complex ice species forming under molecular cloud and protostellar envelope conditions, developing experimental pipelines that integrate *ex-situ* analysis techniques (such as gas chromatography-mass spectrometry) while preserving the sample in vacuum conditions or inert atmospheres for as long as possible becomes increasingly relevant. Finally, with JWST enabling better benchmarking of volatile materials in planet-forming zones, the combined power of observations, experiments, and modeling will be more capable than ever of uncovering the ice composition in disk midplanes, where planet formation is actively underway.